Improvement in Cyclic Stability of Sodium Ion Battery Cathodes through Surface Modification

Abdul Moeez

A thesis
submitted in partial fulfillment of the
requirements for the degree of

Masters of Science in Materials Science and Engineering

University of Washington

2021

Committee:

Jun Liu, Chair

Lucien N. Brush

Guozhong Cao

Program Authorized to Offer Degree:
Materials Science and Engineering

University of Washington

Abstract

Improvement in Cyclic Stability of Sodium Ion Battery Cathodes through Surface Modification

Abdul Moeez

Chair of the Supervisory Committee:
Professor Jun Liu
Department of Materials Science and Engineering

Layered type cathodes used in Sodium Ion batteries are prone to structural degradation as they undergo electrochemical cycling. The structural degradation is the consequence of transition metal dissolution due to unstable or non-uniform cathode-electrolyte interface (CEI), formation of side products like Hydrofluoric acid, formation of new phases in the cathode structure, moisture and carbon dioxide ingression or Jahn-Teller distortion. Some of the approaches used in past employed metal-oxide coatings, electrolyte engineering, replacement of transition metal ions and doping of different elements. However, these strategies were limited to low capacity cathodes. The structural degradation is more prominent in high capacity cathodes like $Na_{0.55}[Ni_{0.1}Fe_{0.1}Mn_{0.8}]O_2$ (NFM) as larger number of Na ions are de-intercalated. Improvement in the cyclic stability of these cathodes remains a challenge. In this thesis, a fluoride based coating has been employed over the cathode particles to prevent the dissolution of transition metals in Localized Highly Concentrated Electrolyte (LHCE) thus maintaining the structural integrity of cathode over longer cycling life. This procedure resulted in capacity retention of 92% over 100 cycles at 0.1C for coated cathode as compared to 76.9% for uncoated cathode. Moreover, X-ray Diffraction (XRD) and Angle Resolved X-ray Photoelectron Spectroscopy (AXPS), revealed that the fluoride coating has been integral in achieving uniform and robust cathode electrolyte interface thus preventing the transition

metal dissolution.

TABLE OF CONTENTS

LIST OF FIGURES

GLOSSARY

ANODE: The electrode in a battery that acts as a host of intercalating ions in full cell while supplies the ions in half cell.

BATTERIES: An electrochemical system primarily consists of cathode, anode, electrolyte and separator.

CATHODE: The electrode that is primarily the host of intercalating in half cell while it supplies the ions in full cells.

CATHODE ELECTROLYTE INTERPHASE: The combination of organic and inorganic species formed when cathode is exposed to electrolyte. It is abbreviated as CEI.

COULOMBIC EFFICIENCY: The ratio of specific discharge capacity and specific charge capacity.

C-RATE: The rate with which battery is charge or discharged relative to its maximum capacity. item[Electrolyte] The medium between anode and cathode that allows diffusion of ions.

GRAVIMETRIC ENERGY DENSITY: Energy stored in a device per unit of its mass. The units of energy density are Wh/kg.

SEPARATOR: A thin membrane placed between the anode and cathode to prevent short circuit while allowing the ion exchange.

SOLID ELECTROLYTE INTERPHASE: The combination of organic and inorganic compounds formed at the surface of electrode when exposed to the electrolyte. It is abbreviated as SEI.

SPECIFIC CAPACITY: The total Amp-hours available per unit mass. The units of specific capacity are mAh/g.

VOLUMETRIC DENSITY: The energy stored in a device per unit of its volume. The units of volumetric density are Wh/L.

ACKNOWLEDGMENTS

The author acknowledges the Coast Salish peoples of this land, the land which touches the shared waters of all tribes and bands within the Duwamish, Puyallup, Suquamish, Tulalip and Muckleshoot nations on whose land this research was performed.

The author acknowledges University of Washington for providing the state-of-the art research facilities to preform this research.

The author acknowledges Prof. Jun Liu for providing the opportunity to work in Liu Laboratory at the University of Washington. This thesis wouldn't have been possible without his mentorship and guidance.

The author also acknowledges the help and mentorship offered by Dr. Xianyong Wu, Dr. Yao Liu, Dr. Xiaoyu Jiang and Dr. Mengyu Yan. The trainings and insights provided by them had been integral for performing this research.

The author acknowledges the help and trainings offered by Dr. Samantha L. Young, Scott Braswell and Ellen Lavoie at Molecular Analysis Facility at the University of Washington.

The author acknowledges support offered by Maria Politi who kept him inspired and motivated throughout the pandemic.

The author acknowledges Fulbright Commission, Institute of International Education (IIE), United States Educational Foundation in Pakistan (USEFP) and Bureau of Education and Cultural Affairs, U. S Department of State for giving author the opportunity to study and complete graduate studies at the University of Washington - Seattle.

Lastly, the author acknowledges their family members and friends who supported the author throughout.

DEDICATION

For my friends, family, mentors and teachers

Chapter 1

INTRODUCTION

Batteries are one of the most ubiquitous and important energy storage devices during present times. From earphones to laptops and from automotive to grid scale energy storage; all these systems employ batteries. The application of battery type for each system dependent on its gravimetric and volumetric energy density. While the gravimetric energy density determines the mass requirement of the system, volumetric density dictates the space required for the battery systems. Since past two decades Lithium Ion (Li-ion) batteries have been ruling in majority of mobile applications. However, last decade has seen an exponential rise in demand of Li-ion batteries.

With the increase in efforts to curb the emissions, world is readily transitioning towards green and sustainable energy resources. To maximize the benefits of these resources, applications like automobiles and grid scale energy storage are required to be electrified. This transition towards greener resources has put world lithium reserves under constraints. With Lithium concentration already limited in the earth's crust, the efforts around the world are focused on exploring the lithium alternative batteries. The relative concentrations of elements in earth's crust are shown in 1.1(a). Moreover, the trend in increasing cost of Li_2CO_3 is shown in 1.1(b).

To meet the supply and demand of Li based energy storage devices, materials alternative to Li have been explored. These materials include Sodium, Potassium, Zinc, Iron, Magnesium etc. Among these sodium (Na) has been considered promising candidate for grid scale energy storage applications owing to the relatively low cost and higher abundance in earth crust. However, issues like low initial Coulombic efficiency, poor cyclic stability, incompatibility between electrode and electrode, phase transformations, non-uniform Solid-Electrolyte

Interphase (SEI) limit the practical and commercial application of these systems. In this thesis, improvement in cyclic stability of layered type Na ion battery cathodes have been explored through LiF coating.

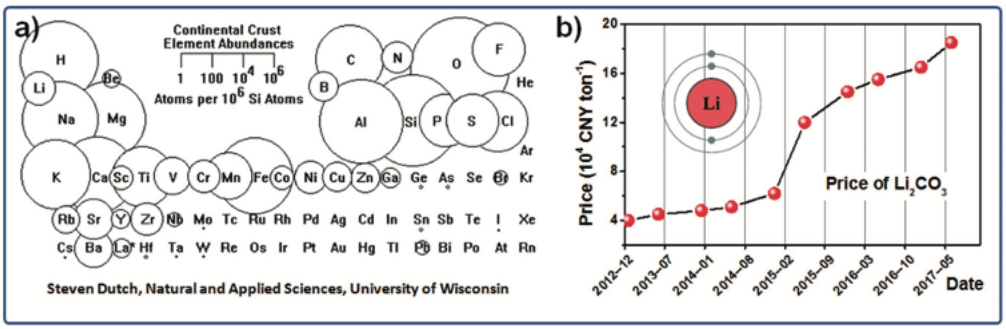

Figure 1.1: (a)Relative abundance of different elements in earth's crust (b)Trend of increasing cost of Li_2CO_3[1]

In the first chapter, Na ion battery cathodes have been introduced. The chapter introduces different kind of cathode materials available and how they've been implemented or processed. The chapter also introduces the Electrolyte engineering used as a tool to improve the electrochemical performance of the Na ion batteries. The third section introduces different strategies explored previously in the domain of Na ion batteries to improve the cyclic stability and the overall electrochemical performances.

The second chapter introduces the methodology and experimentation adopted in this research to improve the electrochemical performance of selected cathode. The third chapter encompasses the discussion on investigation of how our proposed methodology brings advantage to Na ion batteries. Final chapter includes the concluding remarks and explores future research areas for the presented system.

1.1 Working principle of a Battery

Whereas primary batteries in the past utilized one directional chemical reaction to produce electricity as output, the modern secondary batteries can employ either of the two kinds of reversible mechanisms. The conversion mechanism uses reversible chemical reaction to reacts

diffusing ions with the host structures (electrodes) to produce energy. This achieves very high theoretical capacities. [2] The huge change in volume during these reactions makes these system harder to stabilize. The other mechanism is known as intercalation. The intercalation mechanism allows ions to be stored in the lattice spacings of an electrode. Thus when the system is charged, the ions from the cathode (positive electrode) moves towards anode. These ions are then stored in between the interatomic layers or voids. When the system is discharged, these ions move back to the inter-atomic spaces in cathode producing the electronic current in the circuit outside the cell. A schematic of the process is shown in figure 1.2

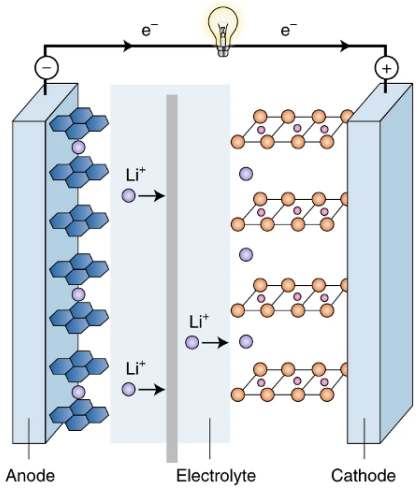

Figure 1.2: Schematic for an intercalation type cell [3]

1.2 Na Ion Battery Cathodes

One of the primary requirements of Na Ion battery cathode is minimal volume change upon intercalation and de-intercalation of Na ion. Minimal volume change contributes to the long term cyclic stability of the cathode material. In terms of coordination, Na prefers six coordination atoms either in Octahedral or Prismatic arrangements. [4] The tetrahedral geometry is uncommon for Na based materials which leads to two major types of cathodes in materials

namely Polyanionic and Layered Oxides.[4] Many of theses electrodes take inspiration from the Li-ion battery systems.

Some of the most popular electrode systems used in Na-ion batteries are fluorides, sulfides, phosphates, and oxides. The types of Na Ion cathode materials on the basis of structure are explained in subsections below:

1.2.1 Polyanionic Type

The polyanionic electrodes for Na ion batteries are composed of series of tetrahedron anion units $(XO_4)^{-n}$ and their derivatives $(X_mO_4)^{-n}$.[5] These materials exhibit high redox potential, high thermal stability owing to the M−O−X interaction and strong oxygen atom linkages respectively. However, the disadvantages of these materials include poor electrical conductivity and low specific capacity. An image of polyanionic $NaFePO_4$ structure is given in figure 1.3.

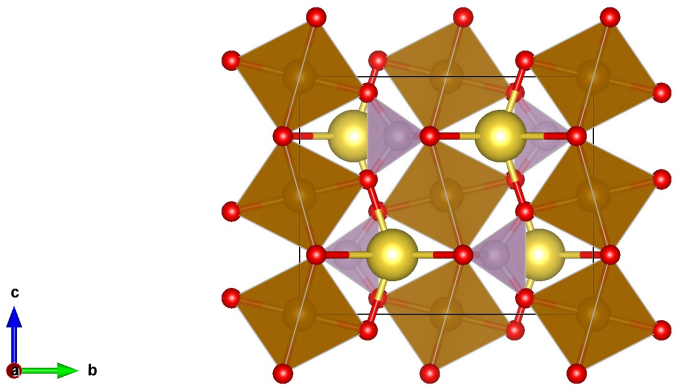

Figure 1.3: Structure of Olivine type $NaFePO_4$[6]

Although $NaFePO_4$ is not thermodynamically stable, it is synthesized using cation exchange from olivine $LiFePO_4$.[5, 7] The olivine structure produces capacity of 125 mAh/g

with average working voltage of 2.7 V. [8] The working voltage in some other olivine structures has been increased through replacement of Fe by other cations like Mn, V, Cr and Ti. The highest specific capacity achieved through this process is 178 mAh/g for $Na_2TiV(PO_4)_3$ with capacity retention of 77% over 500 cycles at 10C. [9] Apart from phosphates, pyrophosphates, mixed phosphates, fluorophosphates, sulfates and silicates have shown promising results over long term cyclic stability. However, the specific capacity for these cathodes remains low. Another factor that impedes the commercialization of polyanionic cathodes is utilization of transition metals like Vanadium. To achieve high capacities and high cyclic stability, most of these cathodes use Vanadium which is expensive as compared to other transition metals.

1.2.2 Layered Metal Oxides Type

Layered metal oxides cathodes have long been popular in Li-ion batteries. While $LiCoO_2$ has been most widely used cathode material in the Li-ion batteries; Nickel, Manganese, Cobalt (NMC) and Nickel, Cobalt, Aluminum (NCA) are some other layered metal oxides which have been extensively assessed for use in automobile and other mobile applications. [10] Since the polyanionic cathodes utilize expensive elements like Vanadium to achieve higher cyclic stability, these cathodes have shown promising results in Na-ion battery chemistry too.

The layered metal oxide cathodes are primarily divided into two main categories depending on the crystal structures. These structures are P (Prismatic) and O (Orthogonal). Various theories for which structure a particular composition will take exists. One proposition regards electronegativity differences between the transition metal oxides while the other proposition attributes cumulative ionic potential between transition metals and Na ions as the reason for determining the crystal structure. [12, 11] The categorization of structures on the basis of ionic potential is shown in fig 1.4

According to Delmas et. al, the alkali metal and transition metal ions, in non-stoichiometric combination, forms different kind of layers depending on the position an alkali metal occu-

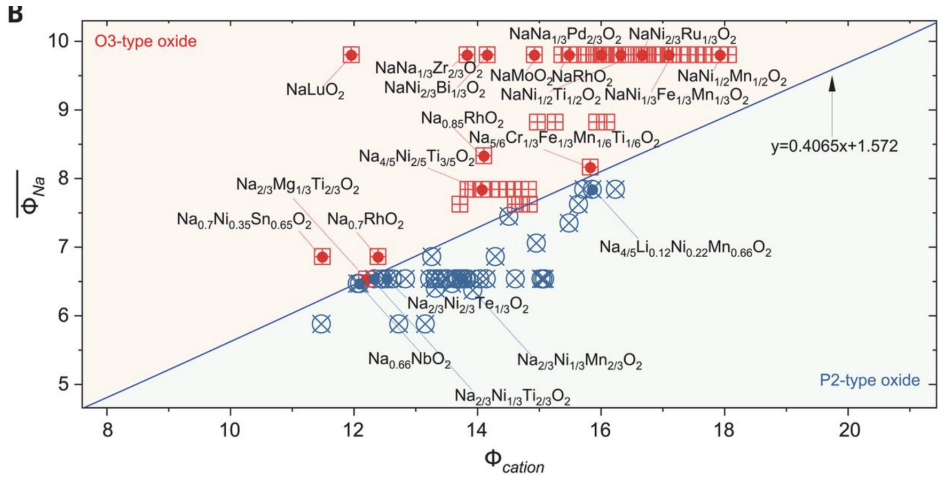

Figure 1.4: Classification of Na-ion battery cathodes using ionic potentials[11]

pies. [12] Each phase contains MO_6 edge sharing octahedral forming $(MO_2)_n$ sheets. [12] Between these sheets, alkali atom occupies either octahedral (O), tetrahedral (T) or prismatic (P) sites.[12] Among these three layered structures, the O-type and P-type dominates the Na-ion cathode structures. The O-type and P-type crystal structures are shown in fig 1.5

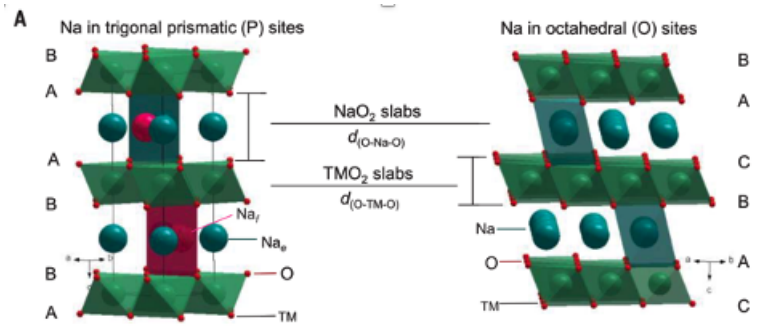

Figure 1.5: O and P type crystal structures in Na-Ion batteries[11]

These two categories are further divided into P2, P′2, O3, O2 and OP4 types. With the layered structure, these cathode provide lower Na diffusion barrier leading to very high specific capacities. Moreover, these cathode structures have higher electrical conductivities unlike their polyanionic counterparts. Apart from these advantages, these cathode structures

suffer from low cyclic stability. One of the reasons from poor electrochemical stability is phase transformation of these cathodes into electrochemically inactive phases. Nucleation and growth of new phases continuously degrade the performance as the cells are cycled.

Oxygen anion reordering is another reason for degradation of cyclic stability. Another factor responsible for degradation of CEI. An incompatible CEI continuously increases the rate of transition metal dissolution, aggravates corrosion and enhances the dead Na metal content. A list of different layered oxide Na ion cathodes with their composition, voltage range, capacity are shown in table 1.1

Table 1.1: List of Layered Oxides

Composition	Voltage Range	Capacity Retention	Max. Specific Capacity	Ref.
$Na[Ni_{0.65}Co_{0.08}Mn_{0.27}]O_2 + AlF_3$	1.5 - 4.1 V	90% after 50 cycles at 75 mA/g	168 mAh/g	[13]
$Na[Ni_{1/3}Fe_{1/3}Mn_{1/3}]O_2$	1.4 - 4.0 V	99% after 150 cycles at 75 mA/g	100 mAh/g	[14]
$Na[Mn_{0.25}Fe_{0.35}Co_{0.25}Ni_{0.25}]O_2$	1.9 - 4.3 V	94% after 20 cycles at C/10	180 mAh/g	[15]
$Na_{0.67}[Mn_{0.65}Co_{0.2}Ni_{0.15}]O_2$	2.0 - 4.4 V	88% after 30 cycles at 20 mA/g	141 mAh/g	[16]
$Na_{0.27}[Mg_{0.11}Mn_{0.89}]O_2$	1.5-4.4 V	60% after 200 cycles at 12mA/g	155 mAh/g	[17]

$Na_{0.78}[Ni_{0.23}Mn_{0.89}]O_2$	2.0 - 4.5 V	86% after 20 cycles at 20 mA/g	138 mAh/g	[18]
$Na_{0.78}[Ni_{0.45}Cu_{0.05}Mn_{0.4}Ti_{0.1}]O_2$	2.0 - 4.0 V	70% after 500 cycles at 1 C	124 mAh/g	[19]
$Na_{0.67}[Mn_{0.65}Ni_{0.2}Co_{0.15}]O_2$	1.5 - 4.2 V	78% after 100 cycles at 120 mA/g	162.3 mAh/g	[20]
$Na_{2/3}[Ni_{1/3}Mn_{2/3}]O_2$	2.0 - 4.5 V	69.6% after 30 cycles at 10 mA/g	162.3 mAh/g	[21]
$Na_{2/3}[Ni_{2/9}Mg_{1/9}Mn_{2/3}]O_2$	2.0 - 4.5 V	83% after 30 cycles at 10 mA/g	145.4 mAh/g	[21]
$Na_{2/3}[Ni_{2/9}Al_{1/9}Mn_{2/3}]O_2$	2.0 - 4.5 V	94.8% after 30 cycles at 10 mA/g	140 mAh/g	[21]
$Na_{2/3}[Ni_{2/9}Fe_{1/9}Mn_{2/3}]O_2$	2.0 - 4.5 V	90.1% after 30 cycles at 10 mA/g	145.8 mAh/g	[21]
$Na_{2/3}[Ni_{2/9}Co_{1/9}Mn_{2/3}]O_2$	2.0 - 4.5 V	85.2% after 30 cycles at 10 mA/g	144.9 mAh/g	[21]
$Na_{0.55}[Ni_{0.1}Fe_{0.1}Mn_{0.8}]O_2$	1.5 - 4.3 V	80% after 500 cycles at 600 mA/g	221.5 mAh/g	[22]

$Na[Ni_{1/3}Fe_{1/3}Mn_{1/3}]O_2$	2.0 - 4.0 V	73% after 500 cycles at 130 mA/g	125 mAh/g	[23]
$Na_{0.5}[Ni_{0.23}Fe_{0.13}Mn_{0.63}]O_2$	1.5 - 4.5 V	80% after 70 cycles at 15 mA/g	210 mAh/g	[24]
$Na_{0.67}[Ni_{0.15}Fe_{0.2}Mn_{0.65}]O_2$	1.5 - 4.3 V	71% after 50 cycles at 13 mA/g	204 mAh/g	[25]
$Na_{2/3}[Ni_{1/3}Mn_{2/3}]O_2 + Al_2O_3$	2.5 - 4.3 V	73.2% after 300 cycles at 86.5 mA/g	160 mAh/g	[26]
$Na_{0.66}[Mn_{0.54}Ni_{0.13}Co_{0.13}]O_2 + Al_2O_3$	2.0 - 4.5 V	66% after 100 cycles at 160 mA/g	123 mAh/g	[27]
$Na_{0.66}[Mn_{0.54}Ni_{0.13}Co_{0.13}]O_2 + ZrO_2$	2.0 - 4.5 V	58% after 100 cycles at 160 mA/g	122 mAh/g	[27]
$Na_{0.66}[Mn_{0.54}Ni_{0.13}Co_{0.13}]O_2 + TiO_2$	2.0 - 4.5 V	61% after 100 cycles at 160 mA/g	106 mAh/g	[27]
$Na_{0.5}[Mn_{0.66}Ni_{0.33}]O_2$ (Cu doping) + MgO	2.0 - 4.5 V	96.45% after 70 cycles at 45 mA/g	131 mAh/g	[28]
$Na[Ni_{0.33}Fe_{0.33}Mn_{0.33}]O_2 + TiO_2$	1.5 - 4.2 V	56.2% after 100 cycles at 20 mA/g	160 mAh/g	[29]

$Na_{2/3}[Mn_{2/3}Ni_{1/6}Co_{1/6}]O_2$ + ZrO_2	2.0 - 4.5 V	91.4% after 100 cycles at 20 mA/g	140 mAh/g	[30]
$Na_{0.65}[Mn_{0.75}Ni_{0.25}]O_2$ + $AlPO_4$	1.5 - 3.75 V	93.7% after 100 cycles at 0.2 C	133.6 mAh/g	[31]
$Na_{0.65}[Mn_{0.75}Ni_{0.25}]O_2$ + $Mg_3(PO_4)_2$	1.5 - 3.75 V	92.4% after 100 cycles at 0.2 C	130.2 mAh/g	[31]
$Na_{0.66}[Mn_{0.9}Ni_{0.1}]O_2$ + Alucone	2.0 - 4.5 V	86% after 100 cycles at 1 C	162 mAh/g	[32]

1.3 Challenges in Layered Type Cathode Materials

Although the layered typer cathode materials are impressive in high discharge capacities, high power densities and low cost, these structures suffer from variety of issues:

1.3.1 Phase Transformations

Both O and P type layered type cathodes suffer from unwanted phase transformations. The phase transformations occurs primarily due to loss of active Na ions. As the cathode is depleted of Na ions, stacking faults are introduced in the structure. As the stacking faults increase, the interslab distances between TMO (transition metal oxide) layers decrease and the capability to host more Na ions decrease. This consequently lead to decrease in capacity of the cathode material. O3 type cathodes are known to be stable over longer cycles, however they are limited by number of Na ions they can donate. The remaining Na ions act as pillars to maintain the interslab distances between TMO layers. P2-type cathodes, which can deliver very high capacities are more prone to structural transformations. An example of phase transformation in O3 and P2 type cathode materials is shown in fig 1.6 & fig 1.7.

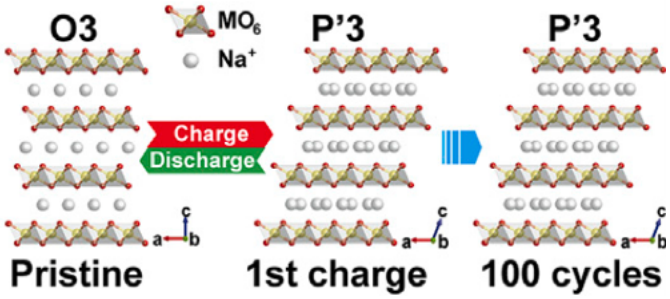

Figure 1.6: Structural evolution of O3 layered cathode during electrochemical cycling[33]

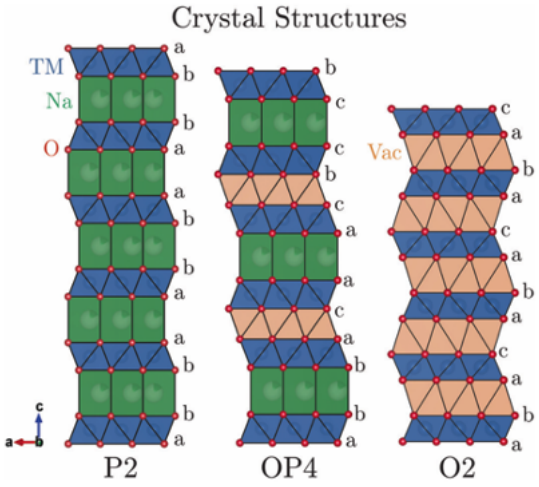

Figure 1.7: Structural evolution of P2 layered cathode during electrochemical cycling[34]

1.3.2 Transition Metal Dissolution

Many Na ion battery systems employing layered type cathodes utilize sodium hexafluorophosphate ($NaPF_6$) or sodium bis(trifluoromethylsulfonyl)imide (NaFSI) as salts for electrolyte. These salts have fluoride groups and are capable of producing hydrofluoric acid (HF) upon hydrolysis. According to Barnes et. al the reaction proceeds as follows [35]:

$$NaPF_6 + H_2O \rightleftharpoons NaF + POF_3 + 2\,HF$$

$$POF_3 + H_2O \rightleftharpoons PO_2F_2{}^- + HF + H^+$$

$$PO_2F_2{}^- + H_2O \rightleftharpoons PO_3F^{2-} + HF + H^+$$

The HF produced through above reactions attack on the the cathode material to dissolve

transition metals. Since the transition metals in layered cathode are integral in maintaining the effective charge between the layers, dissolution of transition metal adds to the structural disability. The overall effect of transition metal dissolution is side reactions and reduction in cyclic stability of Na ion battery.

1.3.3 Jahn-Teller Distortion

Jahn-Teller distortion is transformation of higher symmetry structure into lower symmetry to achiever lower energy state thus reducing the degenerate states. In layered metal oxides, the transition metals like Mn^{2+} or Mn^{3+} are capable to undergo transition from octahedral structure to tetrahedral structure due to higher level of degenerate states. The tetrahedral structure reduces the symmetry along with the energy of the system. Although the transition achieves higher stability for the system, however, as cathode material, it decreases the Na ion conductivity thereby reducing the specific capacity. [36] Previously, doping of different transition metal into the structure of layered cathodes has improved the cycling stability. The doped transition metal replaces Jahn-Teller (JT) active ions like Mn^{3+} or Ni^{3+} and oxidizes these species to reduce distortion. [37]

1.3.4 Moisture and Air Sensitivity

The layered cathode structure, both P and O type structures are prone to structural damage by moisture. Due to high level of sensitivity towards moisture, the handling, storage and processing of cathode powders, inert environments are required at every stage. This increases the cost of processing and fabrication of cell, thus decreasing the economic viability for commercialization.The sensitivity towards moisture and air also restricts the use of aqueous solvents for cathode fabrication. Popular non-aqueous solvents and binders like NMP (N-methyl-2pyrrolidone) and Polyvinylidene fluoride (PVDF) are reported to reduce the Mn oxidation state from +4 to +3, thus contributing to Jahn-Teller distortion effect and consequently leading to the cyclic instability. [38, 39] Another factor through which moisture and air sensitivity degrades the performance is ingression of H_2O molecules between the

transition metal oxide layers. This ingression results in increase the distance between layers thus countering the electrostatic forces which maintain the structure. This enables loss of transition metals, release of oxygen and decrease in number of active Na ions. An example of such structural transition is shown in fig 1.8. The layered cathode $Na_{0.67}MnO_2$ transforms into Buserite structure upon exposure to moisture. This phase is essentially identical to the original structure but has larger lattice constant which allows for oxygen release. [40]

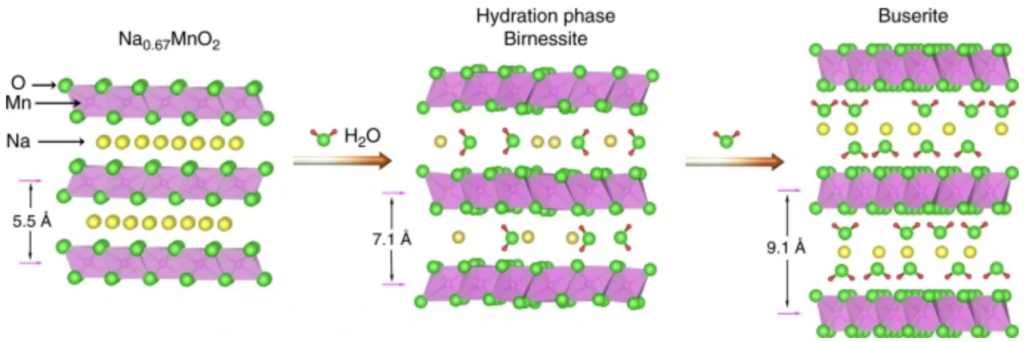

Figure 1.8: Transformation of $Na_{0.67}MnO_2$ into Buserite phase upon exposure to moisture [40]

1.4 Previous Strategies for Improving Cathode Performance

There have been a wide variety of strategies used to improve the electrochemical performance of cathode materials. These strategies are described in subsections below:

1.4.1 Electrolyte Engineering

As described in previous section, the electrochemical performance of battery system hugely relies on the electrolyte. Some of the electrolytes generate Hydrofluoric acid which can cause transition metal dissolutions. Two approaches have been used to improve the cycling performance of cathode materials. First one uses an ultra-low concentration electrolyte while the other used localized highly concentrated electrolyte (LHCE).

Li et. al mapped out the influence of ionic conductivities with the concentration of salt in carbonate based electrolytes. [41] They found that 0.3 M concentration of $NaPF_6$ in EC:DEC provides better cycling stability with with average Columbic efficiency of 99.9% as compared to the 98-99% for electrolyte with 1M concentration. [41] They attributed enhanced cycling performance due to lesser concentration of HF produced during hydrolysis. Moreover, it was reported that these systems provide exceptional performance at temperatures as extreme as -30°C and 55°. This effect was attributed to enhanced kinetics for low concentrations. [41]

Jin et. al used the non-flammable sodium bis(fluorosulfonyl)imide-triethyl phosphate/ 1,1,2,2-tetrafluoroethyl-2,2,3,3-tetrafluoropropyl ether (NaFSI in TEP/TTE) in molar ratio of 1:1.5:2 to achieve highly reversible capacities.[42] They employed LHCE electrolyte for Hard Carbon (HC) Anode and $NaCu_{1/9}Ni_{2/9}Fe_{1/3}Mn_{1/3}O_2$(Na-NCFM). The system achieved high electrochemical stabilities, stable Coulombic efficiencies, and thinner cathode electrolyte interface (CEI). [42] The mechanism of suppression and the cycling performance are shown in fig 1.9 & 1.10.

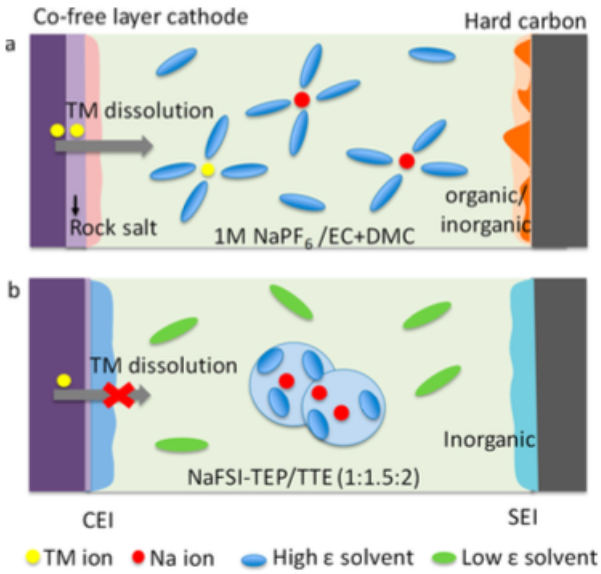

Figure 1.9: Mechanism of suppression of transition metal dissolution suppression in localized highly concentrated electrolyte (LHCE) as compared to conventional carbonate based electrolyte [42]

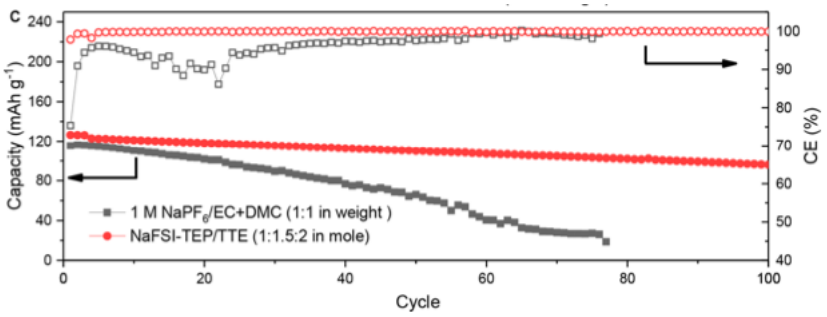

Figure 1.10: Cycling Performance of Na-NCFM || Na in LHCE[42]

Other approaches in electrolyte engineering involved molecular dynamic studies to study solvation structures and addition of additive to inhibit side reactions

1.4.2 Introduction of Pillaring Effect

Since the intercalation type cathodes rely on the extraction of ionic species from the structure, there are limited number of ions available for extraction without the destruction of structure. For O3 type cathodes, the material fails if the sodium concentration falls below 50-60%. For P2 type layered oxides, the limit is 33% which justifies their high capacity. [43] To improve the structural collapse, different metals have been added. One such example is $Na_{0.72}[Li_{0.24}Mn_{0.76}]O_2$. This cathode exhibited very high specific capacity of 210 mAh/g. [44] The exceptional high specific capacity was attributed to oxygen anions reordering thus providing a pillaring effect without destabilizing structure. Though using anions for structure stability makes structure prone to degradation through formation of gases.

Wang et. al created pillar structure using potassium ions and extended the sodium ion extraction range beyond 33%. [43] Through combination of X-ray Photoelectron Spectroscopy (XPS), Inductively Coupled Plasma (ICP) Spectroscopy, Scanning Transmission Electron Spectroscopy (STEM) and X-ray Absorption Fine Structure (XAFS), they reported that small number on electrochemically inactive K^+ ions participate to stabilize the structure when Na^+ are completely extracted. [43]

Apart from alkali metals, the layered cathodes are extensively doped with transition

metals. Cu doped P2-$Na_{0.67}Mn_{0.8}Fe_{0.1}Co_{0.1}O_2$ has shown promising result through increase in interslab distance and decreasing Mn^{3+}/Mn^{4+} ratio. This consequently reduced the Jahn-Teller distortion leading to structural stability. [45] Other elements that have been doped using similar approach include Li, Al, Mg, Ti, Zn and Zr. [46, 47, 17, 48, 49, 50]. Despite extensive studies, cycling stabilities at higher capacities still remain a challenge.

1.4.3 Coating of Cathode Material

Both inorganic and organic coatings have been explored to improve the cycling stability of layered type cathodes. The challenge in both kind remains the ionic conductivity of Na-ion through them. On one end, they coating material inhibits side reactions, gas formation, stabilize CEI and suppress transition metal dissolution, on the other hand, they add to the dead weight of material and decrease the ionic conductivity of Na^+. One of the most popular coating for cathode materials in both Li^+ and Na^+ batteries is Al_2O_3. The strategies used for application of coating involved either mixing the powder with Al_2O_3 or using Atomic Layer Deposition ALD techniques. The later has been effective since it offers better control on thickness of coating.

Liu et. al coated $Na_{2/3}[Ni_{1/3}Mn_{2/3}]O_2$ with Al_2O_3 through wet-chemistry method. They reported 73.3% capacity retention over 300 cycles. [26] Kaliyappan et. al fabricated range of ultra-thin metal oxide coatings on the P2-$Na_{0.66}[Mn_{0.54}Co_{0.13}Ni_{0.13}]O_2$ through atomic layer deposition. They reported TiO_2 as better coating for this cathode as compared to Al_2O_3 and ZrO_2. [27]. Although these cycling stabilities improved for these cathodes but the specific capacities remain on lower end.

Ramasamy et. al combined the doping strategy with MgO encapsulation. Cu doping enhanced the structural stabilities while MgO improved the interfacial kinetics along with increase in cut-off voltages. Again, the specific capacity delivered was 131 mAh/g which remains at the lower end. [28] Jo et. al developed sodium phosphate ($NaPO_3$) coated P2-$Na_{2/3}[Ni_{1/3}Mn_{2/3}]O_2$ via melt impregnation. [51] Through this approach they delayed the decomposition of Mn_2O_3 and induced stability by suppression of oxygen release. The overall

capacity retention was 80% after 50 cycles in half-cell. Therefore, there is still need to improve the cycling stability. Apart from inorganic coating, some organo-metallic coatings like Alucone have also been explored. The coating has been applied through molecular layer deposition and attribute to capacity retention of 86% after 100 cycles at 1C.

Strategies used in Li-ion batteries have been a source of inspiration for other batteries systems like Na, K, Mg and Zn. Among these strategies, surface fluorination has produced promising results. Liu et. al investigated the improvement in cycling performance by coating $LiNi_{0.5}Co_{0.2}Mn_{0.3}$ with LiF.[52] The modified material retained 93.7% of the initial capacity after 100 cycles at 3.0-4.5 V and 0.5C. Moreover, the capacity retention was 81.1% after 300 cycles at 5C. They also reported the average Columbic close to 99.5%. [52] The presence of LiF acts as buffer layer against the formation of HF adding to the high voltage stability. Surface fluorination has also been used in cation disordered rock salt cathodes, Nickel Cobalt Aluminum (NCA), $LiMn_2O_4$, $LiFePO_4$, High Energy Nickel Cobalt Manganese (HE-NCM) and other cathode materials for Li ion batteries to improve the cycling stability. [53, 54, 55, 56]

1.4.4 Challenges in LiF Coating

LiF presence in the Solid-Electrolyte Interface (SEI) has been observed in many cathodes and anodes for Li-ion batteries after electrochemical cycling. The salts used in the electrolyte breaks down in the presence of Li-ions thus enabling the formation of LiF. [57] The presence of LiF on the surface prevents transition metal dissolution on cathode and suppresses formation of dendrites on the anodes. [52, 58] Many attempts have been made to increase the conformity of LiF on the surface of electrodes. One technique involves addition of LiF in the electrolyte to form artificial SEI on the surface of electrodes. [57] However, the poor solubility of LiF in many electrolytes limits the process to achieve high degree of conformal coverage. [59] Without the adequate coverage, the electrodes are prone to parasitic reactions and leads to fracture of the electrode during intercalation and de-intercalation. [59]

Another procedure to achieve conformity utilized reaction between Freon 134a (1,1,1,2-

tetrafluoroethane) and Li metal. The process achieved high cyclic stabilities along with continuous coating with thickness of 40 nm.[59] The only problem in this procedure is that it utilizes Freon 134a which, although non-ozone depleting gas, has a high global warming potential (GWP) and long residence time in atmosphere. The Freon 134a is expected to be phased out in near future which is can cause setback to this process for commercialization.

The advantages of LiF were also observed when Li was incorporated in the layered cathode for Na-ion batteries. [33] The presence of fluorinated species on cathode directly contributed to the suppression of transition metal dissolution thus improving the cyclic stability of the cathode. [33] However, the attempts to develop a conformal coating of LiF and to study its impact o electrochemical performance largely remains unexplored. In an attempt to develop a sustainable procedure to deploy the conformal coating of LiF on high capacity Na-ion battery cathodes, LiDFOB (Lithium Difluoro-oxalato borate) has been used as a precursor for LiF. LiDFOB has been previously used as an additive for electrolyte in Li-ion batteries and it produces LiF upon decomposition during electrochemical cycling. [60] To improve the conformity further, instead of in-situ development of LiF in an electrochemical cell, a liquid phase coating strategy followed by calcination has been used in this research. This processing strategy allowed for better control on the chemical composition and thickness of LiF since other entities like impurities from salt and electrolyte species are absent.

Furthermore, the system used in this research utilizes NaFSI based localized highly concentrated electrolyte (LHCE). The electrolyte system as previously explained is known to suppress the transition metal dissolution but it has only been tested for low capacity cathodes. Herein, we use P2-type $Na_{0.55}[Ni_{0.1}Fe_{0.1}Mn_{0.8}]O_2$ (NFM) cathode which can deliver high capacities at high average voltages.

Chapter 2

METHODOLOGY

For improvement in cyclic stability of Na ion battery system, the first step was selection of cathode material with highest specific capacity. Following the literature review done in previous chapter the material suitable for our need was P2-type $Na_{0.55}[Ni_{0.1}Fe_{0.1}Mn_{0.8}]O_2$ (NFM). This material delivered specific discharge capacity of 221.2 mAh/g at 12 mA/g and 30°C. The material retained 79% of initial discharge capacity after 100 cycles at 60 mA/g and exhibited high average voltage of 2.9 V. The procedure for powder fabrication, coating preparation and characterization are described in sections below.

2.1 Cathode Powder Fabrication

The cathode powder was fabricated using acetate salts of Iron, Manganese and Nickel. The salts were procured from Sigma-Aldrich with purity level of 99.99%. For Na source, Sodium Carbonate (Na_2CO_3) was used. The Manganese Acetate, Nickel Acetate and Sodium Carbonate were grinded in pestle and mortar in air. These powders were transferred inside the glove box where Iron Acetate was mixed. The powders were then pelletized under infrared lamp with 4 metric tons of load over 10 mm diameter die. The pellets were quickly transferred to tube furnace. The pellets were then calcined at 950°C for 12 hours. The ramp rate to reach 950°C was kept 5°C/min. A schematic for powder processing for NFM is shown is fig 2.1.

The samples after calcination were quickly transferred to argon filled glovebox. To make electrodes, the powder was mixed with KETJEN BLACK (KB) carbon and PVDF in ratio of 0.85:0.10:0.05. NMP was used as dilutent to make the slurry. The slurry was mixed for 30 minutes in a Thinky Mixer. The slurry was then applied to aluminum foil with a doctor

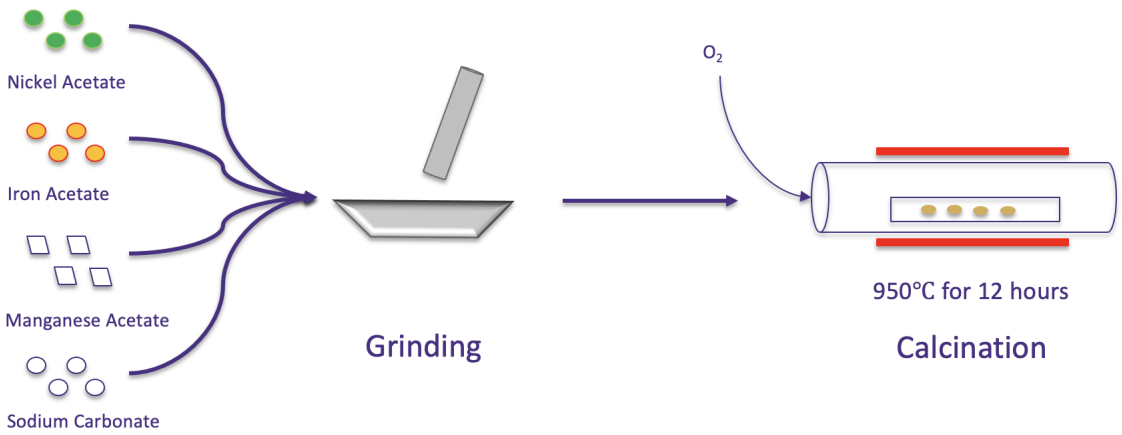

Figure 2.1: Powder processing steps in fabrication NFM powder

blade having thickness 0.35 mm. The electrode was then dried for 24 hours at 120°. The electrode was then punched into discs of 10 mm in diameter. The schematic explaining the process is shown in fig 2.2. The average mass loading obtained was 3.2 mg/cm^2 with standard deviation of 0.36 mg/cm^2.

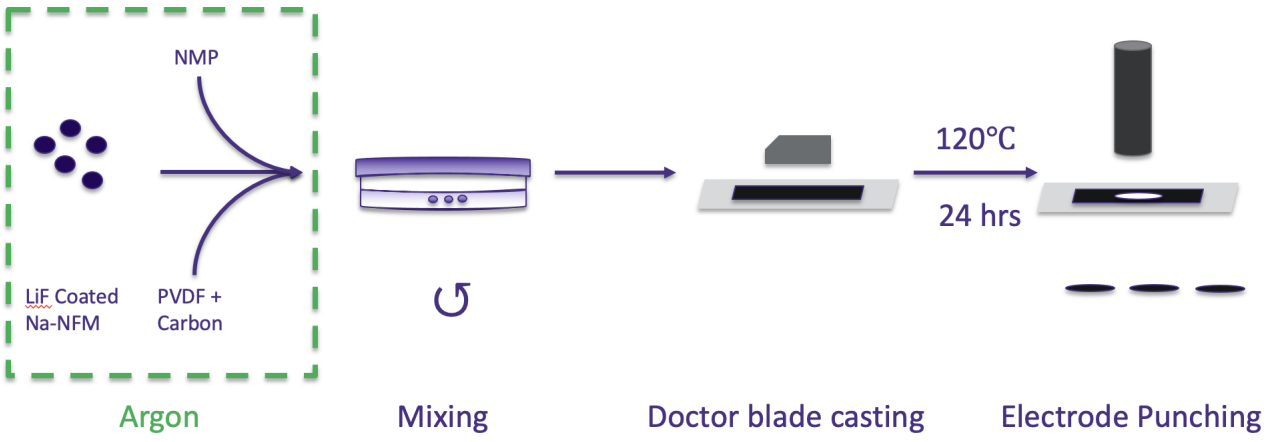

Figure 2.2: Electrode fabrication process

2.2 Application of Lithium Fluoride Coating

To apply the lithium fluoride coating over NFM powder, various concentration by weight of Lithium dioxalatoborate (LiDFOB) were dissolved in 1 mL of methanol. The solution was stirred for 15 minutes over a magnetic stirrer. The concentrations used were 2%, 3%, 4% and 5% by weight of NFM. The respective labels for these concentration are LiF-NFM2, LiF-NFM3, LiF-NFM4 and LiF-NFM5. After stirring, the NFM was added to the solution. 1 mL of methanol was subsequently was added to immerse powder completely in the solution. The dispersion was then stirred at 110°C until all the methanol was evaporated. The paste obtained was transferred to vacuum oven at 80°C for further drying. After 15 minutes, the powder was taken out, and calcined in air at 600°C for 3 hours. The schematic for the coating process is shown in figure 2.3 For electrode fabrication, similar procedure was adopted as described in section 2.1.

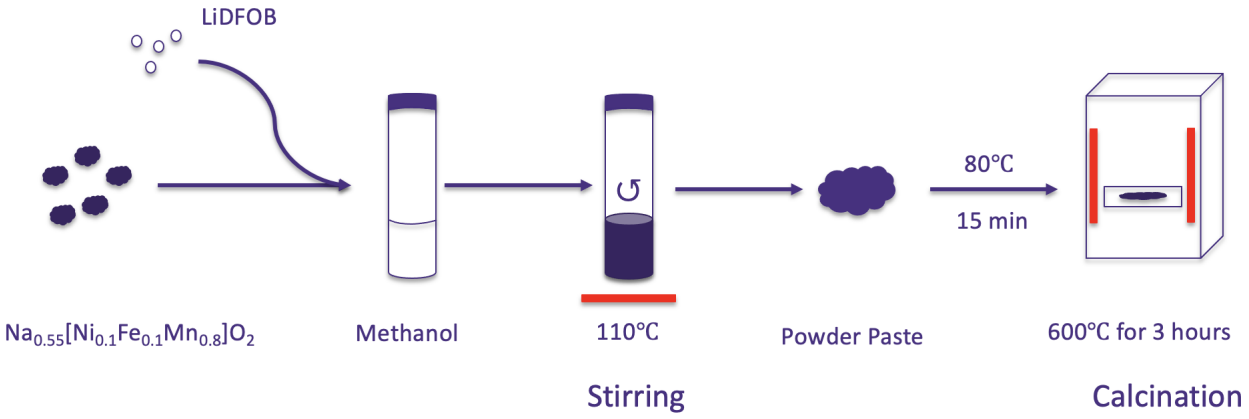

Figure 2.3: Coating process of LiF on NFM powders

2.3 Electrolyte Preparation

The electrolyte preparation involved dissolution of NaFSI in Tri-ethyl Phosphate (TEP) over a magnetic stirrer. The solution was stirred for 24 hours. The 1,1,2,2-tetrafluoroethyl-2,2,3,3-tetrafluoropropyl ether (TTE) was added to make localized highly concentrated electrolyte.

The molar ratio between all three entities was kept as 1:1.5:2. To remove moisture from the electrolyte, freshly cut sodium metal was added to the electrolyte. The sodium was replenished multiple times until the tarnishing effect of electrolyte was taken over.

2.4 Electrochemical Measurements

The 2032 coin cell standard was used for all half coin cells while for the full cells 2016 was used. The electrolyte volume used was 40 μL. The pressure to press the coin cell was kept as 50 kg/cm^2. The H2015 Celgard separator was used for all half cells, while glass fiber separator was used for full cell. For full cell, the Hard Carbon (HC) Anode was pre-sodiated at 0.1 C (20 mA/g). Two different strategies were used for pre-sodiation of HC Anode. In one scenario, the pre-sodiation was stopped in a charged state. This pre-sodiated HC anode had very little Na ions embedded between the layers. In the other scenario, the pre-sodiation was stopped in the discharged state. This pre-sodiated anode was loaded with Na-ions and acted in analogous manner to the sodium foil. The capacity of anode was matched to 1.15 times the capacity of cathode. All the cells were tested on Newware Battery Tester CT-4008-5V10mA at 25°C. The Electrochemical Impedance Spectroscopy (EIS) was performed on two electrode coin cell configuration using GAMRY Interface 1010E.

2.5 Structural and Compositional Analysis

X-Ray diffraction analysis was performed on the Bruker D8 Discover with IμS 2-D diffractometer. The collimator diameter was kept as 0.5 mm for all samples. To avoid the fluorescence generated by transition metals, especially by Fe content, the detector discriminator was set at 7600 eV threshold. The Rietveld refinement for the samples was performed using FullProf Suite and GSAS-II. Scanning electron microscopy was performed using Sirion XL30 with Oxford Instruments Energy Dispersive Spectrometer (EDS) system. Transmission Electron Microscopy (TEM) was performed on Tecnai G2 F20 SuperTwin. For TEM sample preparation, 5 mg of powder was dispersed in 10 mL of Anhydrous Ethanol (200 Proof). The solution was sonicated for 1 hour in two steps of 30 minutes each. The solution

was rested for 20 minutes before being transferred to the glovebox where a droplet of solution was transferred on TEM grid. The excess solution on grid was allowed to evaporate in Argon atmosphere under $H_2O < 0.01$ ppm and $O_2 < 0.01$ ppm. X-ray Photoelectron Spectroscopy (XPS) was performed using Surface Science Instruments S-Probe X-ray Photoelectron Spectrometer. Three spots of each sample were selected to evaluate the spectrum. Samples for all structural and compositional analysis remain sealed in argon until transferred to analysis chamber.

Chapter 3

RESULTS AND DISCUSSION

3.1 X-Ray Diffraction Analysis

The XRD pattern to confirm the true phase of NFM powders is shown in fig 3.1. The Rietveld refinement is also shown in the same figure. The initial parameters for Rietveld refinement were obtained from previously cited literature. [22] The results are in agreement with the structure belonged to hexagonal $P63/mmc$ space group. Moreover, there is little difference between the literature values and measured values for lattice constants. The difference is shown in table 3.1

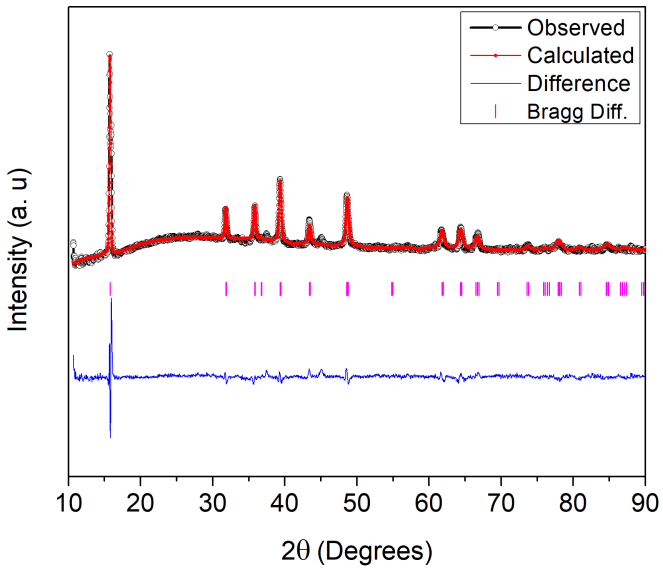

Figure 3.1: Obtained XRD Pattern for as processed NFM along with Refinement

The difference in refinement values primarily arises from the oxygen content in the mate-

rial processed in the lab. The refinement results predict occupancy of 1.3 for oxygen atoms against 1.2 for the literature value. It should be noted that XRD technique is not considered reliable to predict oxygen occupancy or vacancy concentration and these results need to be precisely evaluated through the neutron diffraction technique.

Table 3.1: Comparison between literature values and measure values for lattice constants of NFM

Lattice Constant	Literature Value (Å)	Measured Value (Å)	Percentage Difference
a	2.90194	2.89360	0.28%
c	11.26010	11.23868	0.19%

To verify the change in crystal structure for coated NFM, the procedure was repeated for NFM coated with 2% of LiF precursor. The XRD pattern is shown in figure 3.2. Since there was no obvious peak detected for LiF deposition, the NFM parameters were used for refinement. The refinement is also shown in 3.2.

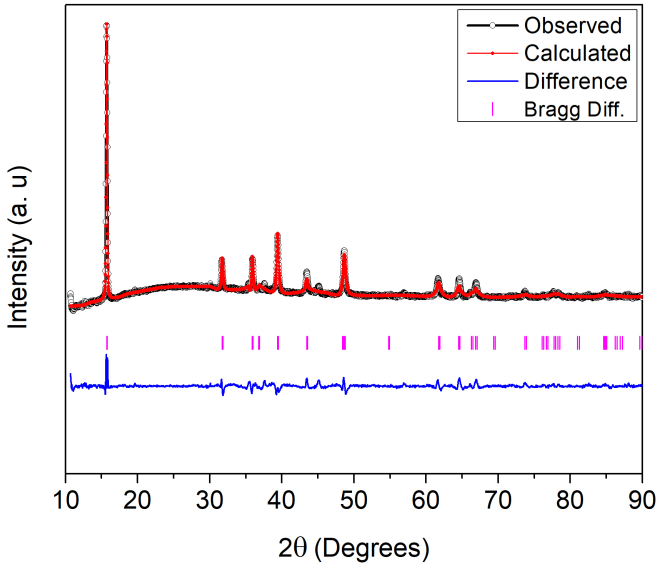

Figure 3.2: Obtained XRD Pattern for as processed LiF coated NFM along with Refinement

To evaluate any changes in lattice parameters, the Rietveld refinement was used to calculate the lattice parameters. The percent differences between measure values and literature values are provided in table 3.2. It should be noted that the lattice parameter 'a' contracted while 'c' expanded. This is in direct correlation with decrease in oxygen occupancy to 1.13. The decrease in occupancy and change in lattice parameters is due to the high temperature calcination to convert LiDFOB to LiF.

Table 3.2: Comparison between literature values and measure values for lattice constants for LiF coated NFM

Lattice Constant	Literature Value (Å)	Measured Value (Å)	Percentage Difference
a	2.90194	2.88632	0.53%
c	11.26010	11.27140	0.10%

3.2 Scanning Electron Microscopy

The images obtained from scanning electron for pristine NFM, LiF-NFM2 and LiF-NFM5 are shown in figure 3.3. The pristine samples clearly show layered structures clumped together. It was observed that there was no morphological difference between NFM and LiF-NFM2. However, morphology of LiF-NFM5 was different with clear roughness on the surface. The EDS maps for NFM, LiF-NFM2 and LiF-NFM5 are shown in figure 3.4. It is evident that the elements have very uniform distribution in the particles. It should be noted that the fluorine signature for LiF-NFM2 is well below the EDS detection limit therefore, it doesn't appear in maps. The presence of fluorine was confirmed using XPS in the next section.

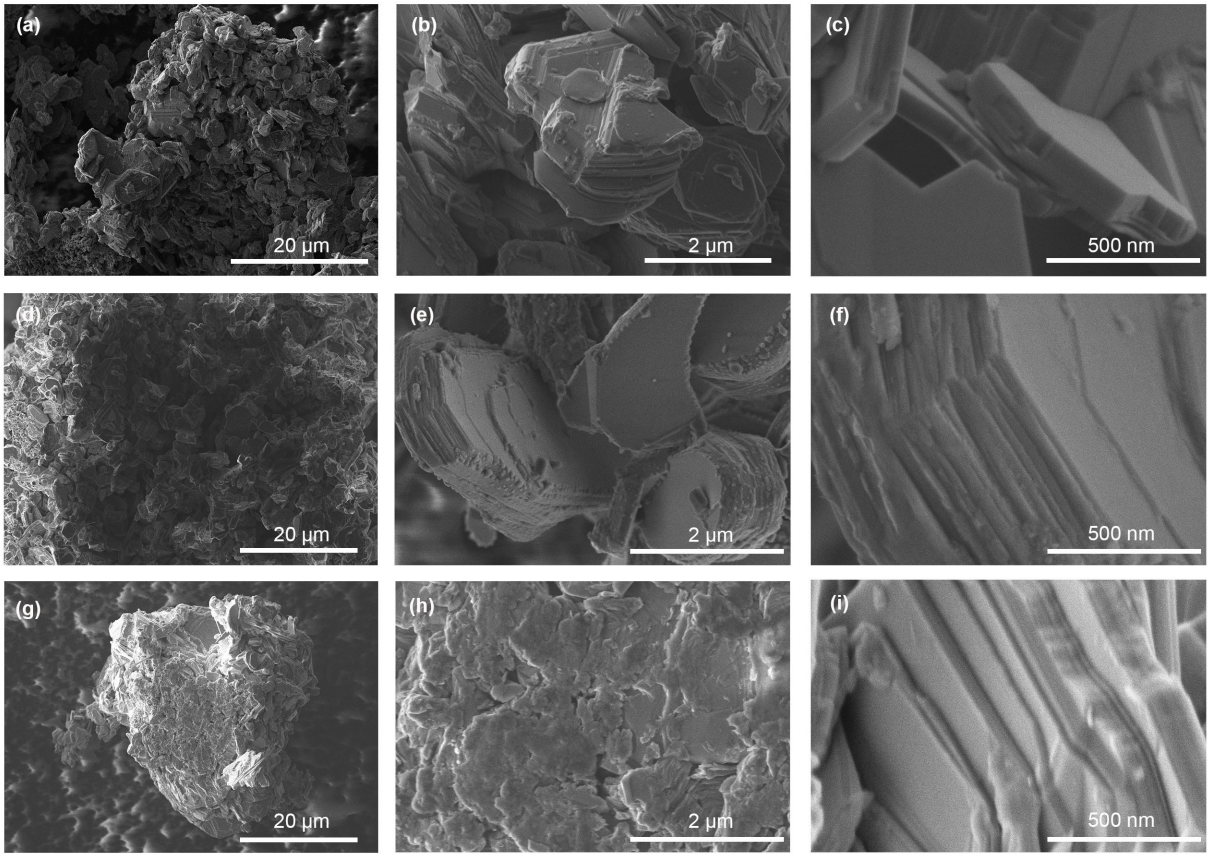

Figure 3.3: SEM Images for (a-c) NFM, (d-f) LiF-NFM2, (g-i) LiF-NFM5

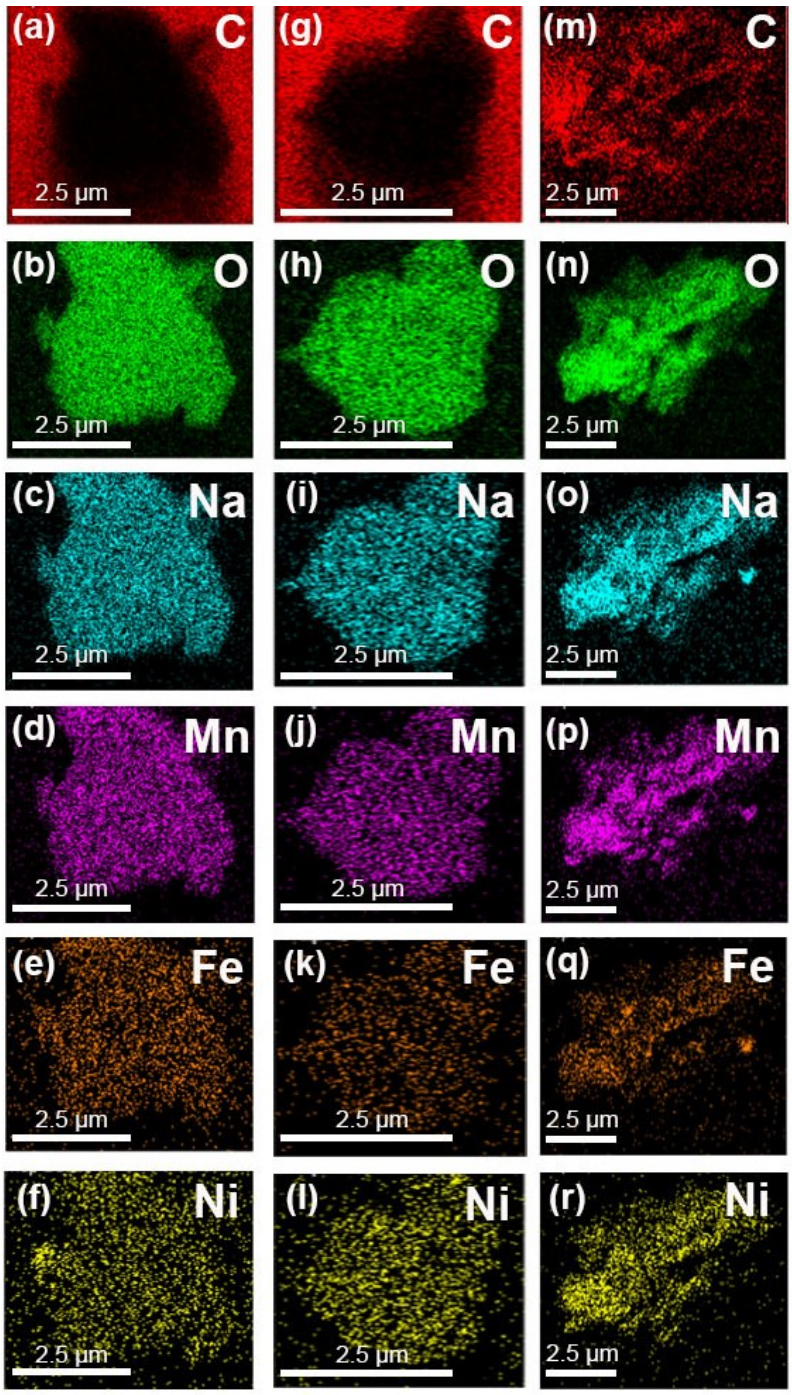

Figure 3.4: EDS Maps for distribution of C, O, Mn, Fe, Ni in (a-f) NFM, (g-l) LiF-NFM2, (m-r) LiF-NFM5

3.3 Transmission Electron Microscopy

To evaluate the conformity of coating over the NFM particles, TEM was performed. The TEM images are shown in figure 3.5. It can be observed from figure 3.5 (a)-(d) that the surface of the layered structure does not contain any coating. The absence of coating on LiF-NFM3 confirms the low conformity of LiF coating. The coating became more pronounced in LiF-NFM5 and showed higher degree of conformity with thickness of 9.6 nm.

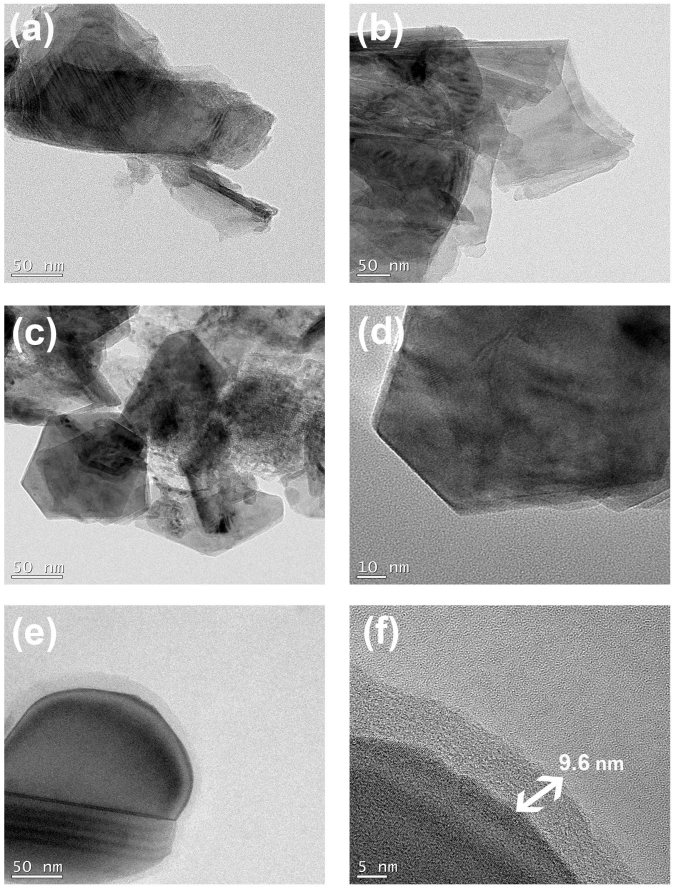

Figure 3.5: Transmission electron microscopy (TEM) images for (a-b) NFM, (c-d) LiF-NFM3, (e-f) LiF-NFM5

3.4 X-Ray Photoelectron Spectroscopy

The XPS spectrums obtained for NFM, LiF-NFM2, LiF-NFM5 are shown in fig 3.6. The NFM spectrum doesn't show any fluorine signature however both LiF-NFM2 and LiF-NFM5 had fluorine in it. Furthermore, the fluorine spectrum was fitted with LiF peak. The peak appearing at 685 eV indicates the presence of metal fluoride (LiF) present on the surface of the LiF-NFM2 and LiF-NFM5 samples. The measured and fitted spectrum for Lithium fluoride is shown in figure 3.7.

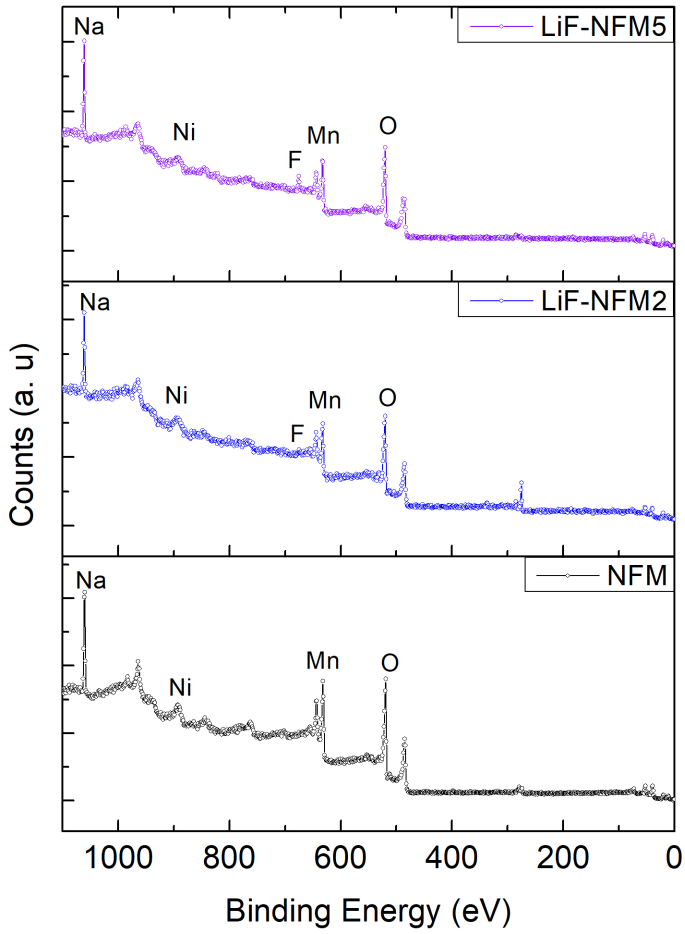

Figure 3.6: XPS Spectra for NFM, LiF-NFM2 and LiF-NFM5

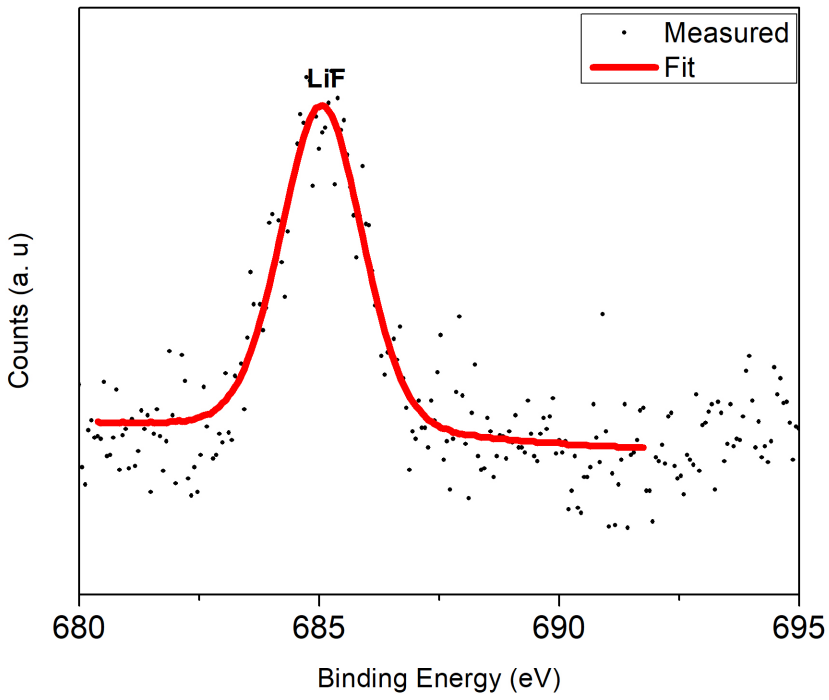

Figure 3.7: High Resolution Measured and fitted XPS spectra for LiF

To further elucidate any changes in the oxidation state, Mn high resolution was analyzed. The high resolution spectra of Mn in NFM, LiF-NFM2 and LiF-NFM5 are shown in figure 3.8. It was observed that due to the presence of LiF on the surface of NFM particles the Mn^{+3} and Mn^{+4} spectra shifts towards higher binding energies which shows and increase in oxidation state. The increase in oxidation state signifies reduction in Jahn-Teller distortion in material. The peak shift data is shown in table 3.3. Although, the crystal structure of materials remains same from coating, the oxidation state increases at the surface which improves the performance of the cathode.

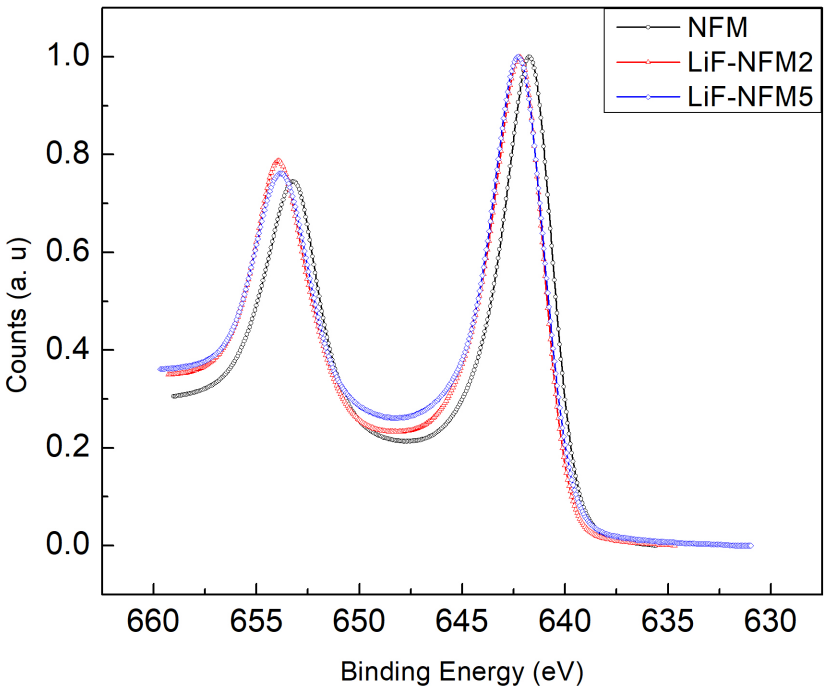

Figure 3.8: High Resolution Mn XPS spectra for NFMNFM, LiF-NFM2 and LiF-NFM5

Table 3.3: Peak shift data for high resolution XPS spectrum for Mn

Cathode	$Mn^{3+/4+}$ Peak 1 (eV)	$Mn^{3+/4+}$ Peak 2 (eV)
NFM	641	653.24
LiF-NFM2	642	653.89
LiF-NFM5	642	653.89

3.5 Electrochemical Testing

The comparison of cyclic stabilities, Columbic efficiencies (%), and selected charge discharge profiles for NFM and LiF-NFM2 are shown in figure 3.9. The LiF-NFM2 cathode evidently performed superior than the NFM cathode. Moreover, the Columbic efficiencies in figure 3.9(b) for LiF-NFM2 are below 100% however, Columbic efficiencies of NFM exceeded 100% for various cycles. This electrochemical behavior signifies side reactions happening on the NFM cathode.

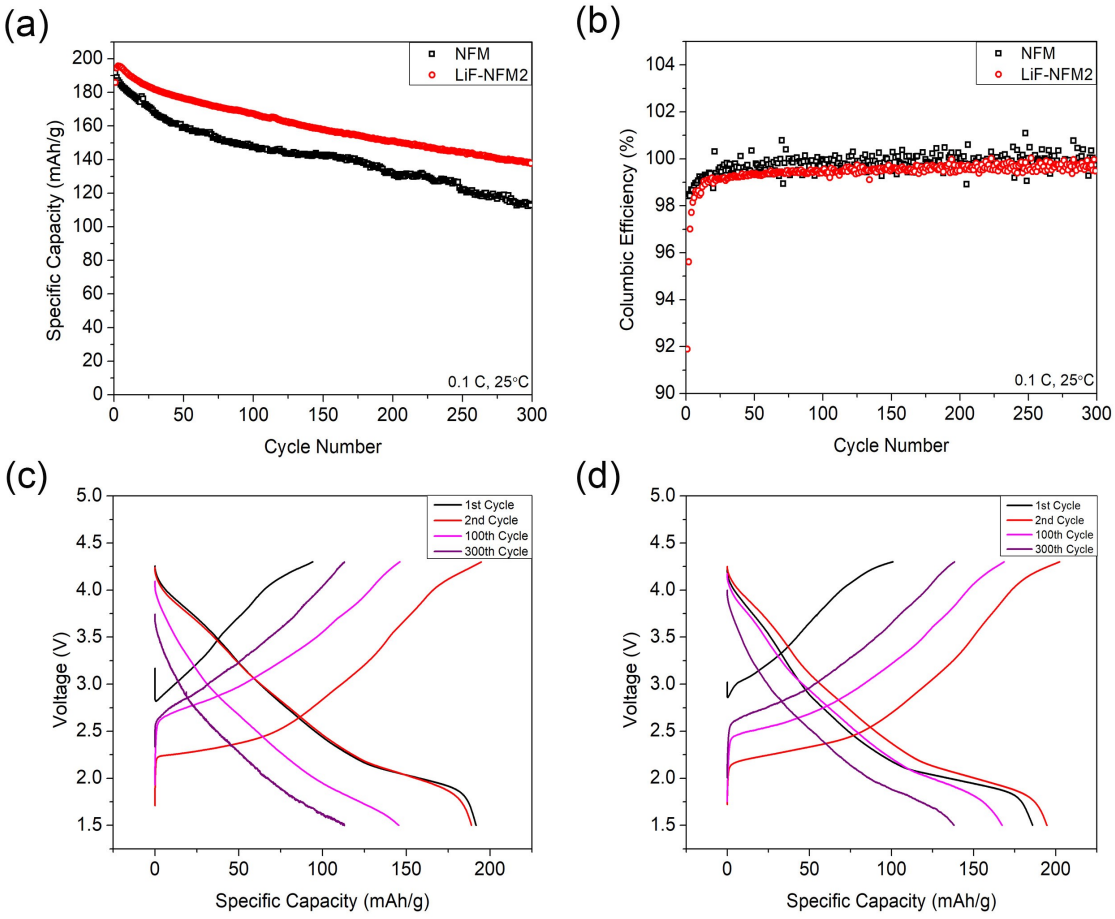

Figure 3.9: (a) cyclic stability comparison between NFM and LiF-NFM (b) Columbic Efficiencies for NFM and LiF-NFM (c) Selected charge-discharge curves for NFM (d) Selected charge-discharge curves for LiF-NFM

Moreover, in NFM charge-discharge profiles, the specific capacity decreases after first cycle however, in LiF-NFM2 the capacity increases for second cycle. Furthermore, as the cycle number increase the voltage decrease increases. The 300th discharge cycle starts with 3.75 V as compared to charging voltage of 4.3 V. The drop is evident in figure 3.9(c). For LiF-NFM2, the 300th discharge cycle starts with 4.0 V as shown in figure 3.9(d). This drop in voltage could be due to transition metal dissolution and it was evident in both cathodes. However, the LiF-NFM2 showed more stability than the NFM. The rate capabilities for NFM, LiF-NFM2, LiF-NFM3, LiF-NFM4 and LiF-NFM5 are shown in figure 3.10.

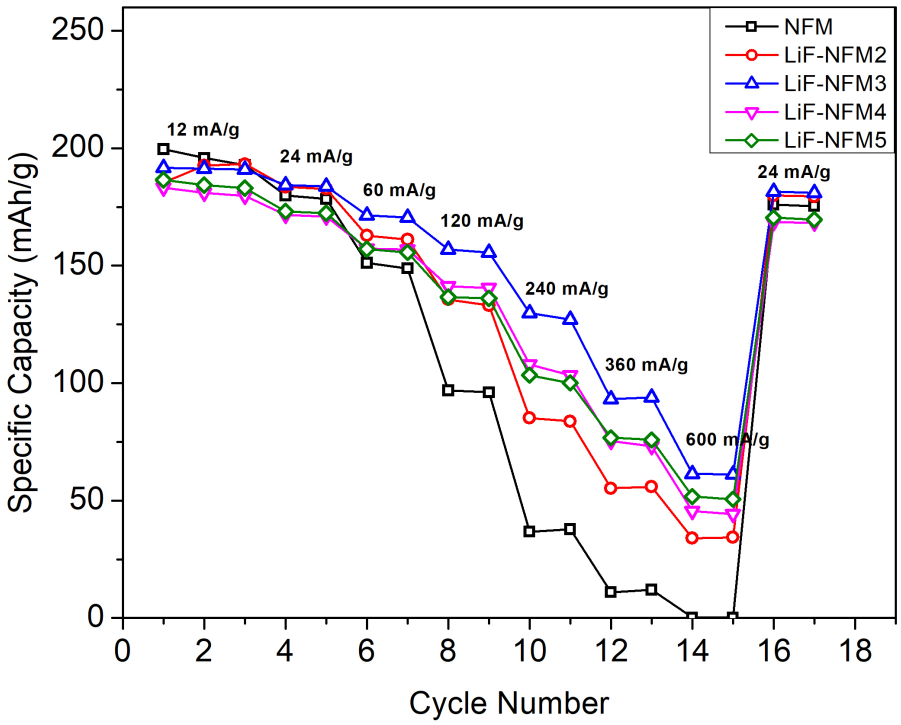

Figure 3.10: Rate capability for NFM, LiF-NFM2, LiF-NFM3, LiF-NFM4 and LiF-NFM5

It is evident that specific capacities decrease as the weight percentage of coating increase. Moreover, LiF coating also improved the specific capacities at high C-rates. To evaluate the cyclic stabilities at higher C-rates, the cathodes were evaluated at 0.3 C. The cyclic performance is shown in figure 3.11. Similar, to previous results, the LiF coated cathodes have higher cyclic stabilities as compared to the NFM.

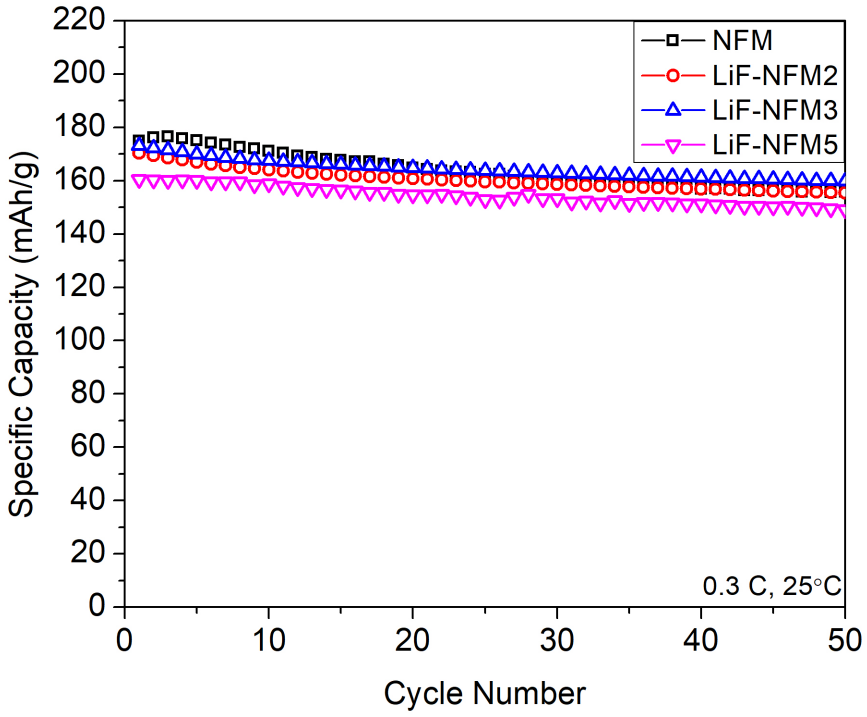

Figure 3.11: Cyclic stabilities for NFM, LiF-NFM2, LiF-NFM3 and LiF-NFM5 at 0.3 C

3.6 Electrochemical Impedance Spectroscopy and cyclic Voltammetry

To further evaluate the performance enhanced by LiF coating on the cathodes, the Electrochemical Impedance Spectroscopy (EIS) was performed on NFM, LiF-NFM2, LiF-NFM3 and LiF-NFM5. The EIS results are shown in figure 3.12. These results indicate a decrease in charge transfer resistance with increase in coating thickness when the LiF precursor is increased from 0% to 3%. However, when the amount of LiF precursor was increased to 5% by weight the charge transfer resistance increases. Since, LiF is poor Na ion conductor, increasing the coating thickness increase the charge transfer resistance as well.

To further elucidate whether Li ions are involved in intercalation or not, Cyclic Voltammetry (CV) was performed at 0.2 mV/s scan rate. The results are shown in figure 3.13. No additional peak was detected in CV scan for LiF-NFM2 as compared to NFM. This indicates

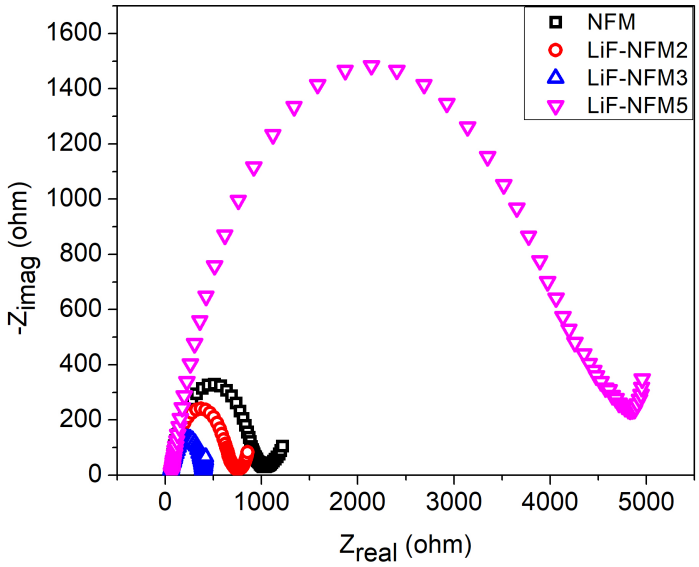

Figure 3.12: Electrochemical Impedance Spectroscopy for NFM, LiF-NFM2, LiF-NFM3 and LiF-NFM5

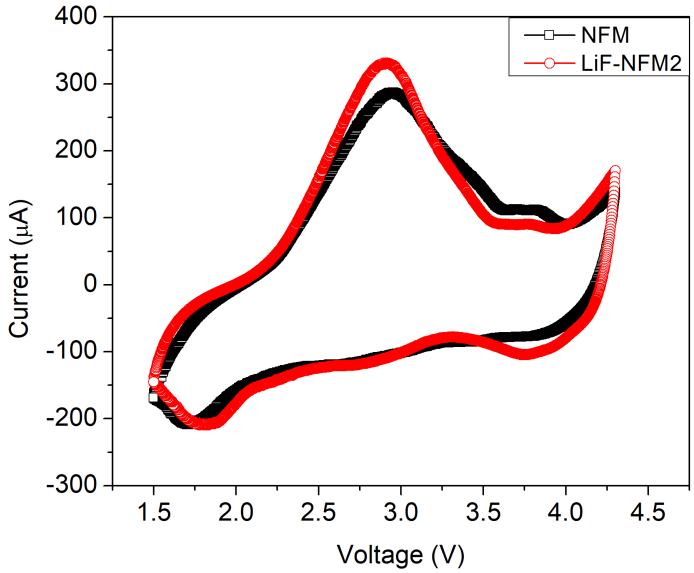

Figure 3.13: Cyclic Voltammogram for NFM and LiF-NFM2

that the Na ions are the only intercalating specie for the coated cathodes. The only difference that appeared in Cyclic Voltammogram was increase in peak current. The peak current for LiF-NFM2 was 325.7 μA while for NFM2 was 286.9 μA. The result is consistent with the EIS studies which showed that the interfacial resistance for the ions decreases as the result of LiF coating.

3.7 Post Electrochemical cyclic Evaluation

To further investigate the chemical and structural changes happening on the electrode during cyclic, SEM, XRD and XPS was carried out. The results for scanning electron microscopy are shown in figures 3.14, 3.15 & 3.16. The electrodes were cycled for 100 cycles at 0.3 C and 25°. Morphologically, there was no difference between the cycled NFM and LiF-NFM2. Both electrodes were found to have regions of pulverization on the surface when compared to pristine electrodes. Therefore, both electrodes equally suffered from electrochemical cycling.

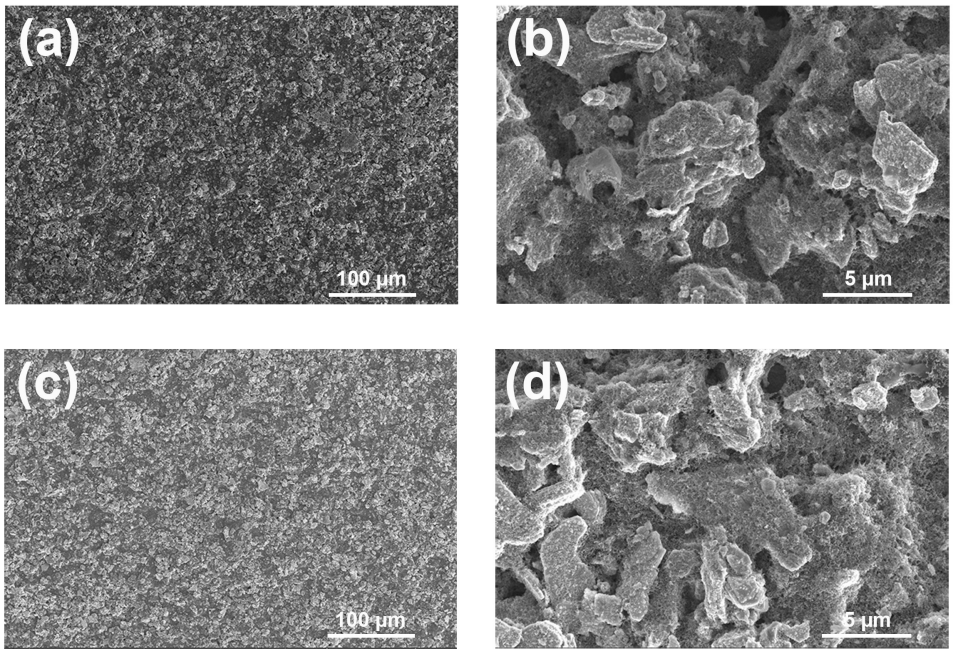

Figure 3.14: SEM images for (a-b) Pristine NFM (c-d) Cycled NFM (e-f) Pristine LiF-NFM2

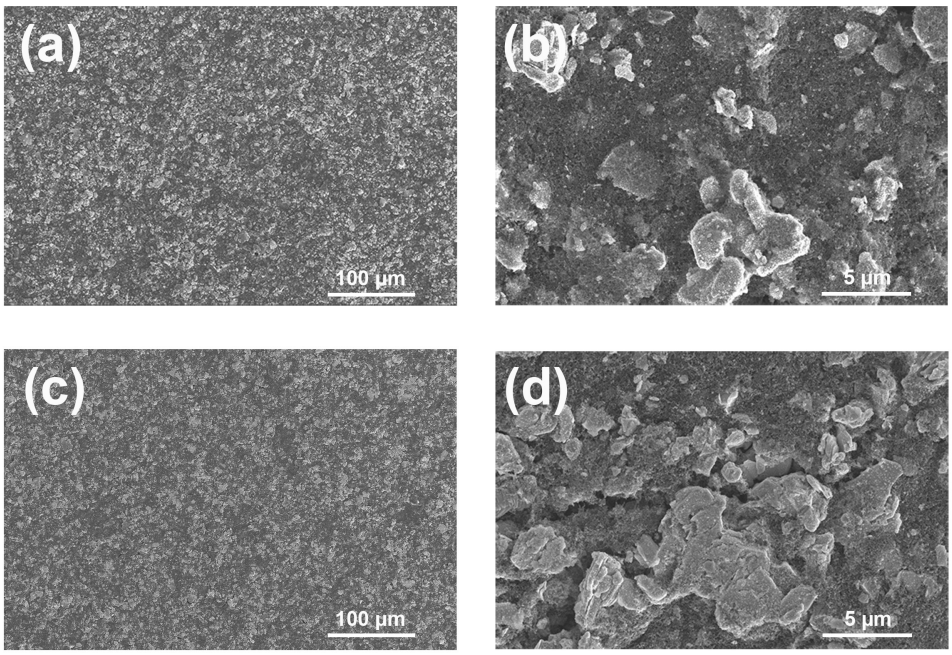

Figure 3.15: SEM images for (a-b) Pristine LiF-NFM2 (c-d) Cycled LiF-NFM2 (i-j)

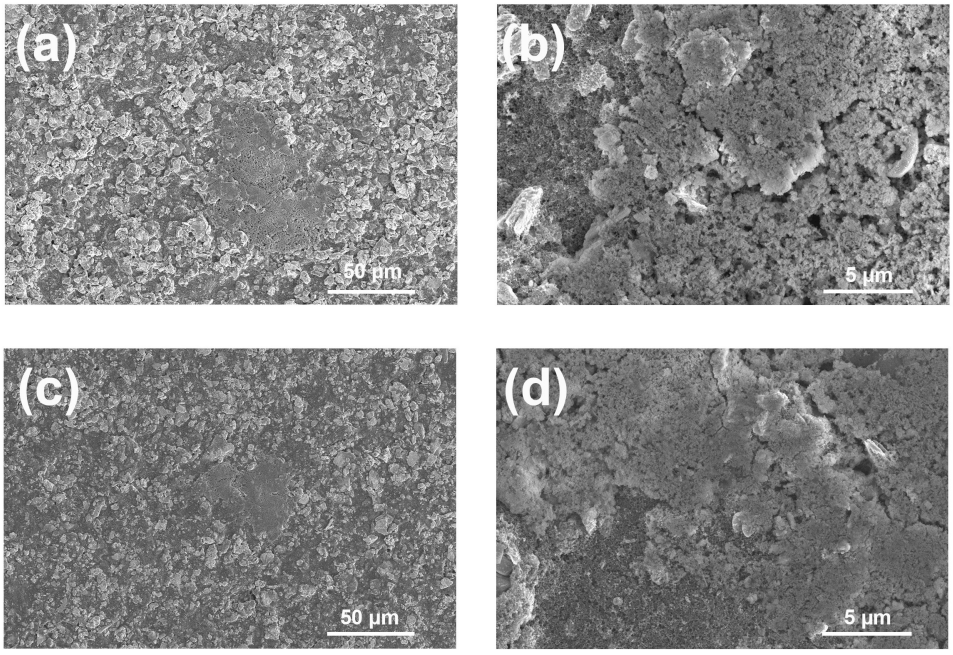

Figure 3.16: SEM images for (a-b) Pulverization of particles in cycled NFM (c-d) Pulverization of particles in cycled LiF-NFM2

The XRD pattern for cycled NFM, LiF-NFM2 and LiF-NFM5 are shown in figure 3.17. All the samples see a shift in 2θ values towards higher angle which relates the decrease in Na-ions as the cycle number increases thus reducing the inter-atomic spacing. Moreover, the peak intensities change indicates nucleation and growth of monoclinic phases P'2 in the structure. It should be noted that 2θ shift in LiF coated cathodes was smaller as compared to the uncoated cathode. Furthermore, XRD pattern for LiF-NFM5 showed little change in relative peak intensities as compared to the other cathodes. This indicates the increase in structural stability with increase in LiF content. The 2θ values for pristine and cycled cathodes are shown in table 3.4

Table 3.4: Comparison between 2θ values for pristine and cycled cathodes

Cathode	$2\theta_{1p}$ Pristine	$2\theta_{2p}$ Pristine	$2\theta_{2p} - 2\theta_{1p}$	$2\theta_{1c}$ Cycled	$2\theta_{2c}$ Cycled	$2\theta_{2c} - 2\theta_{1c}$
NFM	15.64	31.64	16.00	15.88	32.21	16.24
LiF-NFM2	15.66	31.66	16.00	15.82	31.98	16.16
LiF-NFM5	15.62	31.62	16.00	15.88	32.04	16.16

It is evident from table 3.4 that the difference between two peaks becomes larger upon electrochemical cycling for all cathodes. This signifies a change in lattice spacing since active Na is being lost. However, the difference in two peaks is greater for NFM as compared to LiF-NFM2 and LiF-NFM5. Thus LiF coating on NFM, although not completely, prevents structural degradation to some extent.

To further evaluate the positive impact of LiF coating on the electrochemical performance of NFM cathodes, the cycled cathodes were analyzed using angle resolved XPS (AXPS). In AXPS, the sample angle is rotated at different angles to observe chemical composition at different depths. The three configurations used for the cycled sample in AXPS are shown in

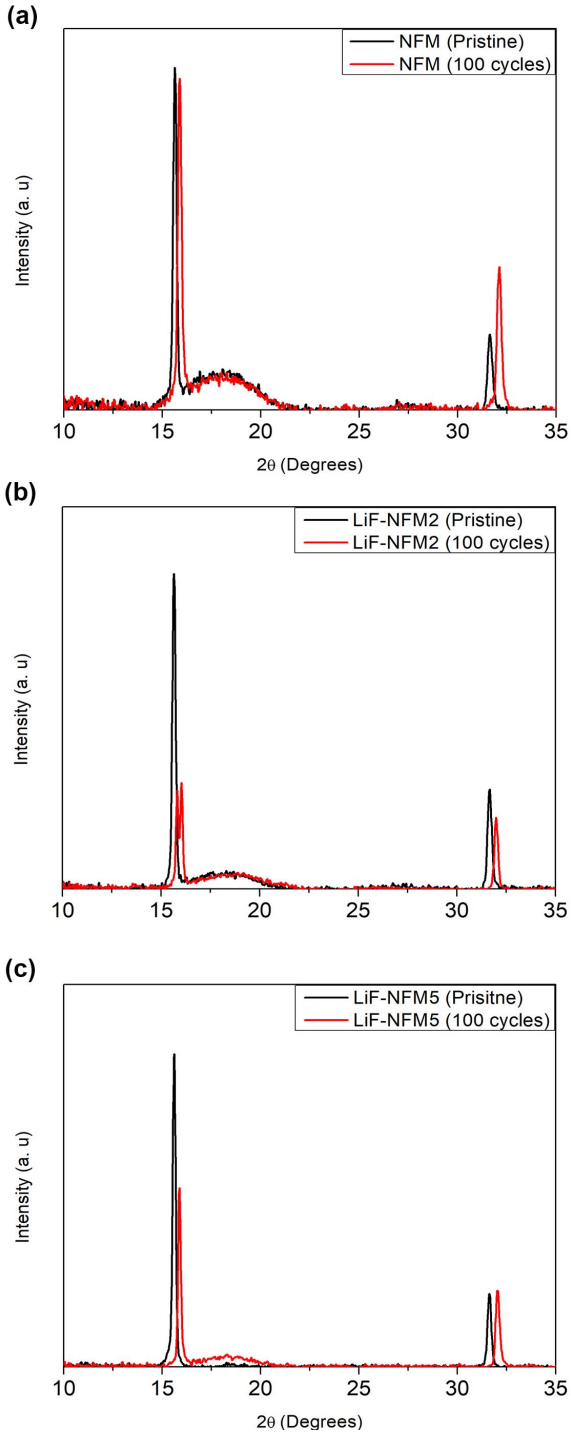

Figure 3.17: XRD Pattern for (a) NFM, (b) LiF-NFM2 and (c) LiF-NFM5 after 100 cycles at 0.3 C in comparison to their pristine cathodes

figure 3.18. The corresponding depth for 0°, 55° and 75° is 10 nm, 5 nm and 1nm, respectively. The AXPS spectra for cycled NFM and cycled LiF-NFM2 are shown in figure 3.19 (a) & (b).

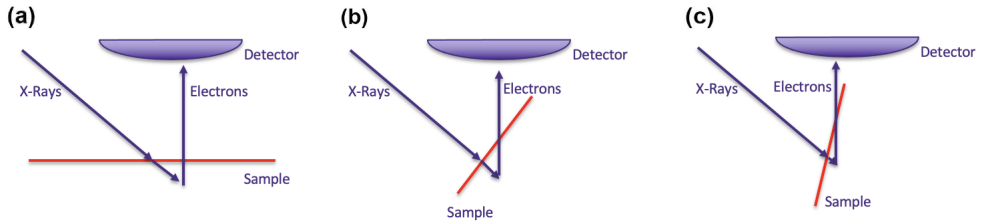

Figure 3.18: AXPS sample configuration for (a) 0°, (b) 55° and (c) 75°

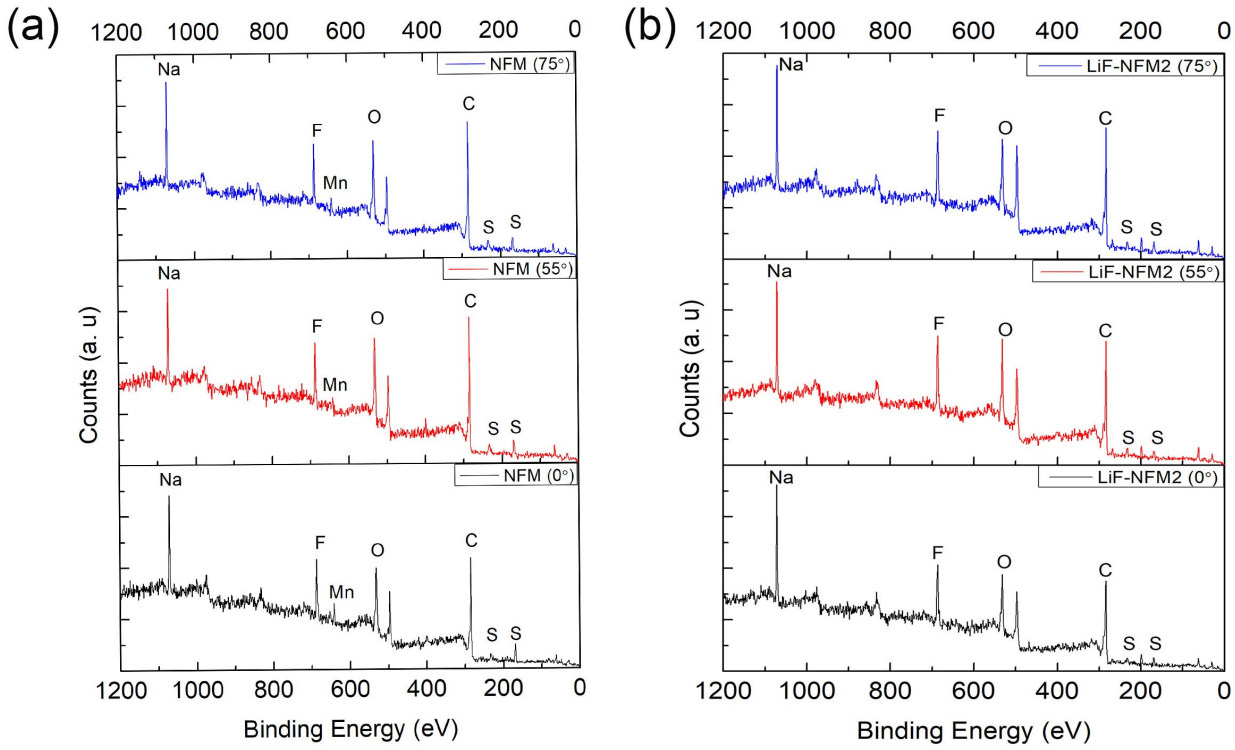

Figure 3.19: XPS Survey Spectrum after 10 cycles at 0.1 C for (a) NFM (b) LiF-NFM2

For cycled NFM, the CEI was found to be composed of Mn along with Na, F, O, C and S. The Mn spectra was present for all depths in NFM. However, all the depths scanned

on LiF-NFM2 showed no signs of transition metal. The reason behind absence of Mn from the AXPS spectra in LiF-NFM2 is high ion migration energies for transition metal ions. The LiF present on the surface of NFM acts as barrier for transition metal dissolution and prevents the scavenging attack from the electrolyte on cathode particles. The spectra in AXPS also exhibits that the CEI produced over the LiF-NFM2 during cyclic is more durable and uniform.

3.8 Full-Cell Electrochemical Performance

The electrochemical performance for LiF-NFM2 vs. Hard Carbon (HC) anode is shown in figure 3.20. The HC anode was already sodiated but stopped in charged state, so it had little amount of intercalated Na ions. The capacity of the system in this case is determined by Na ions which came from the cathode. As evident the cyclic stability is not very superior as compared to the half-cell performance. After 100 cycles at 20 mA/g, the capacity retention was 83% of initial discharge capacity. Moreover, the average Columbic efficiency for the system corresponded to 94%. This relates to the significant loss of active Na ions. Unlike half-cell in which sodium metal foil can replace lost Na ions, the electrochemical performance cannot be replicated in full cell since there is no Na ion reservoir available.

There are number of factors which contribute to the low Columbic efficiency and poor cyclic stability. The most prominent one is anode. Despite persistent efforts to improve the Columbic efficiency of anode, the results have not been satisfactory. Moreover, even the widely used anode like HC displays poor stability when coupled with the LHCE. The possible reasons behind this effect is low cyclic stability and Columbic efficiency of HC in LHCE.

Another factor that contributes to the Columbic efficiency is the separator. Most common separator composed of sandwich layers of Polyethylene-Polypropylene-Polyethylene is designed for Li-ion batteries. These separators work well with smaller ionic size however, performs poorly when used in systems like Na-ion. The pores and surface area of separator restricts the Na ion exchange and reduces the performance. Another common separator,

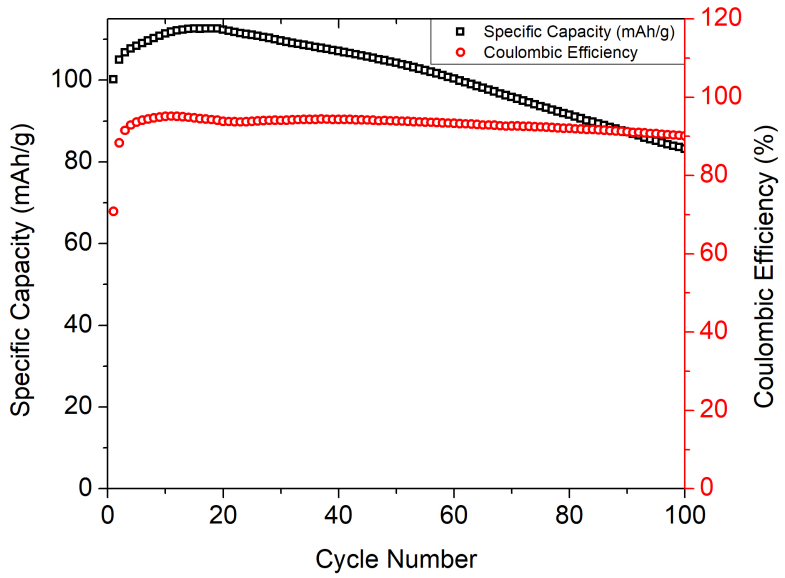

Figure 3.20: Electrochemical performance of LiF-NFM2 vs. HC

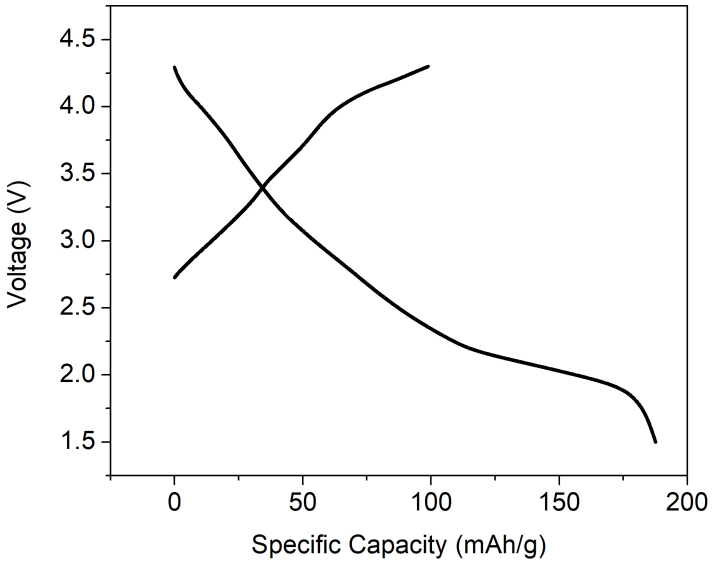

Figure 3.21: Charge discharge curve for first cycle of Li-NFM2 vs. sodiated HC

glass fiber, has higher porosity and has shown promising results in the literature. The separator, although compatible with HC anode, was found incompatible with the NFM cathode in LHCE. The glass fiber induced certain electrochemical transitions at low voltages which were not present in half-cell or reference literature. The results for low voltage electrochemical transitions in half-cell with glass fiber are given in figure A.1.

The charge discharge curve for fully sodiated HC is shown in figure 3.21. The specific capacity for LiF-NFM2, delivered on the basis of cathode, was 187 mAh/g at 12 mA/g and 25°C. The performance at low c-rate is comparative of the half-cell electrochemical performance. However, extensive cycling is required to further validate the viability of the approach.

Chapter 4

CONCLUSION

A facile synthesis procedure has been presented in this thesis to improve the cyclic stability of high capacity cathodes for Na ion batteries. The LiF coating produced through this procedure evidently improved the cyclic stability of NFM cathodes. The best performance achieved was for LiF-NFM2 and LiF-NFM3. The LiF-NFM2 was tested at 0.1 C for 300 cycles. These conditions corresponds to the testing time of 6,000 hours. Most of the published research cites testing at higher C-rates which clouds the side reactions thus achieving high cyclic stabilities at the cost of lower specific capacities. After 100 and 300 cycles, LiF-NFM2 retained 90% and 70% of the initial discharge capacity, respectively. The NFM2 from 100 and 300 cycles retained 76.9% and 58.7% of the initial discharge capacity, respectively. The capacity retention after cycled at 600 mA/g for LiF coated NFM was above 98% while for uncoated NFM it was found to be 97%. Moreover, rate performances of LiF coated cathodes was found to be superior than uncoated cathode.

The improved performance was due to improved charged transfer resistance by LiF coating. The XRD performed on cycled electrodes revealed greater structural change for uncoated cathodes as compared to the LiF coated cathode. The AXPS was used to validate the cause behind improved electrochemical performance and better structural integrity. AXPS revealed presence of Mn in the CEI of NFM cathode at the depths of 10 nm, 5 nm and 1 nm. This exhibits the Mn dissolution behavior in the uncoated cathodes. The CEI for LiF coated cathodes was free from Mn which relates to improved structural stability for these cathodes. The TEM studies revealed poor conformity of LiF for NFM cathode with low concentration of precursor. However, when the precursor concentration was increased to 5%, the conformity increased. The LiF-NFM5 analysis showed coating thickness close to 10 nm however,

since the LiF is poor conductor of Na ions, the coating compromised the specific capacity and charge transfer resistance. Therefore, to further improve the performance of NFM cathode a process for better conformity and lower coating thickness needs to be devised.

Owing to the success of LiF coated electrodes in half-cell, the cathodes were tested against hard carbon anode. The cyclic stability for LiF-NFM2 cathode against HC was found to be poor and only 80% of initial capacity after 100 cycles was retained. This poor performance in the full cell requires need for better anode and separator for Na-ion batteries. Only then the Na ion batteries would be economically viable for commercialization.

REFERENCES

[1] Xiaodong Hong, Jun Mei, Lei Wen, Yueyu Tong, Anthony J Vasileff, Liqun Wang, Ji Liang, Ziqi Sun, and Shi Xue Dou. Nonlithium metal–sulfur batteries: steps toward a leap. *Advanced materials*, 31(5):1802822, 2019.

[2] Seung-Ho Yu, Xinran Feng, Na Zhang, Jeesoo Seok, and Héctor D Abruña. Understanding conversion-type electrodes for lithium rechargeable batteries. *Accounts of chemical research*, 51(2):273–281, 2018.

[3] John B Goodenough. How we made the li-ion rechargeable battery. *Nature Electronics*, 1(3):204–204, 2018.

[4] Michael D Slater, Donghan Kim, Eungje Lee, and Christopher S Johnson. Sodium-ion batteries. *Advanced Functional Materials*, 23(8):947–958, 2013.

[5] Ting Jin, Huangxu Li, Kunjie Zhu, Peng-Fei Wang, Pei Liu, and Lifang Jiao. Polyanion-type cathode materials for sodium-ion batteries. *Chemical Society Reviews*, 49(8):2342–2377, 2020.

[6] Anubhav Jain, Shyue Ping Ong, Geoffroy Hautier, Wei Chen, William Davidson Richards, Stephen Dacek, Shreyas Cholia, Dan Gunter, David Skinner, Gerbrand Ceder, and Kristin a. Persson. Commentary: The Materials Project: A materials genome approach to accelerating materials innovation. *APL Materials*, 1(1):011002, 2013.

[7] Philippe Moreau, Dominique Guyomard, Joël Gaubicher, and Florent Boucher. Structure and stability of sodium intercalated phases in olivine $FePO_4$. *Chemistry of Materials*, 22(14):4126–4128, 2010.

[8] Seung-Min Oh, Seung-Taek Myung, Jusef Hassoun, Bruno Scrosati, and Yang-Kook Sun. Reversible $NaFePO_4$ electrode for sodium secondary batteries. *Electrochemistry Communications*, 22:149–152, 2012.

[9] Dongxue Wang, Xiaofei Bie, Qiang Fu, Ditty Dixon, Natalia Bramnik, Yong-Sheng Hu, Francois Fauth, Yingjin Wei, Helmut Ehrenberg, Gang Chen, et al. Sodium vanadium titanium phosphate electrode for symmetric sodium-ion batteries with high power and long lifespan. *Nature communications*, 8(1):1–7, 2017.

[10] N Omar, P Van den Bossche, G Mulder, M Daowd, JM Timmermans, J Van Mierlo, and S Pauwels. Assessment of performance of lithium iron phosphate oxide, nickel manganese cobalt oxide and nickel cobalt aluminum oxide based cells for using in plug-in battery electric vehicle applications. In *2011 IEEE Vehicle Power and Propulsion Conference*, pages 1–7. IEEE, 2011.

[11] Chenglong Zhao, Qidi Wang, Zhenpeng Yao, Jianlin Wang, Benjamín Sánchez-Lengeling, Feixiang Ding, Xingguo Qi, Yaxiang Lu, Xuedong Bai, Baohua Li, et al. Rational design of layered oxide materials for sodium-ion batteries. *Science*, 370(6517):708–711, 2020.

[12] Claude Delmas, Claude Fouassier, and Paul Hagenmuller. Structural classification and properties of the layered oxides. *Physica B+ c*, 99(1-4):81–85, 1980.

[13] Ho-Hyun Sun, Jang-Yeon Hwang, Chong Seung Yoon, Adam Heller, and C Buddie Mullins. Capacity degradation mechanism and cycling stability enhancement of AlF_3-coated nanorod gradient $Na[Ni_{0.65}Co_{0.08}Mn_{0.27}]O_2$ cathode for sodium-ion batteries. *ACS nano*, 12(12):12912–12922, 2018.

[14] Donghan Kim, Eungje Lee, Michael Slater, Wenquan Lu, Shawn Rood, and Christopher S Johnson. Layered $Na[Ni_{1/3}Fe_{1/3}Mn_{1/3}]O_2$ cathodes for na-ion battery application. *Electrochemistry Communications*, 18:66–69, 2012.

[15] Xin Li, Di Wu, Yong-Ning Zhou, Lei Liu, Xiao-Qing Yang, and Gerbrand Ceder. O3-type $Na[Mn_{0.25}Fe_{0.25}Co_{0.25}Ni_{0.25}]O_2$: A quaternary layered cathode compound for rechargeable na ion batteries. *Electrochemistry communications*, 49:51–54, 2014.

[16] Dingding Yuan, Wei He, Feng Pei, Fayuan Wu, Yue Wu, Jiangfeng Qian, Yuliang Cao, Xinping Ai, and Hanxi Yang. Synthesis and electrochemical behaviors of layered $Na_{0.67}[Mn_{0.65}Co_{0.2}Ni_{0.15}]O_2$ microflakes as a stable cathode material for sodium-ion batteries. *Journal of Materials Chemistry A*, 1(12):3895–3899, 2013.

[17] Daniel Buchholz, Christoph Vaalma, Luciana Gomes Chagas, and Stefano Passerini. Mg-doping for improved long-term cyclability of layered na-ion cathode materials-the example of p2-type $Na_xMg_{0.11}Mn_{0.89}O_2$. *Journal of Power Sources*, 282:581–585, 2015.

[18] Chuze Ma, Judith Alvarado, Jing Xu, RaphaeÃàle J CleÃÅment, Moses Kodur, Wei Tong, Clare P Grey, and Ying Shirley Meng. Exploring oxygen activity in the high energy p2-type $Na_{0.78}Ni_{0.23}Mn_{0.69}O_2$ cathode material for na-ion batteries. *Journal of the American Chemical Society*, 139(13):4835–4845, 2017.

[19] Hu-Rong Yao, Peng-Fei Wang, Yue Gong, Jienan Zhang, Xiqian Yu, Lin Gu, Chuying OuYang, Ya-Xia Yin, Enyuan Hu, Xiao-Qing Yang, et al. Designing air-stable o3-type cathode materials by combined structure modulation for na-ion batteries. *Journal of the American Chemical Society*, 139(25):8440–8443, 2017.

[20] Zheng-Yao Li, Rui Gao, Limei Sun, Zhongbo Hu, and Xiangfeng Liu. Designing an advanced p2-$Na_{0.67}Mn_{0.65}Ni_{0.2}Co_{0.15}O_2$ layered cathode material for na-ion batteries. *Journal of Materials Chemistry A*, 3(31):16272–16278, 2015.

[21] Wenwen Zhao, Hideyuki Kirie, Akinobu Tanaka, Masashi Unno, Shinji Yamamoto, and Hideyuki Noguchi. Synthesis of metal ion substituted p2-$Na_{2/3}Ni_{1/3}Mn_{2/3}O_2$ cathode material with enhanced performance for na ion batteries. *Materials Letters*, 135:131–134, 2014.

[22] Jang-Yeon Hwang, Jongsoon Kim, Tae-Yeon Yu, and Yang-Kook Sun. A new p2-type layered oxide cathode with extremely high energy density for sodium-ion batteries. *Advanced Energy Materials*, 9(15):1803346, 2019.

[23] Hong Wang, Xiao-Zhen Liao, Yang Yang, Xiaomin Yan, Yu-Shi He, and Zi-Feng Ma. Large-scale synthesis of $NaNi_{1/3}Fe_{1/3}Mn_{1/3}O_2$ as high performance cathode materials for sodium ion batteries. *Journal of The Electrochemical Society*, 163(3):A565, 2016.

[24] Ivana Hasa, Daniel Buchholz, Stefano Passerini, Bruno Scrosati, and Jusef Hassoun. High performance $Na_{0.5}[Ni_{0.23}Fe_{0.13}Mn_{0.63}]O_2$ cathode for sodium-ion batteries. *Advanced Energy Materials*, 4(15):1400083, 2014.

[25] Dingding Yuan, Xiaohong Hu, Jiangfeng Qian, Feng Pei, Fayuan Wu, Rongjun Mao, Xinping Ai, Hanxi Yang, and Yuliang Cao. P2-type $Na_{0.67}Mn_{0.65}Fe_{0.2}Ni_{0.15}O_2$ cathode material with high-capacity for sodium-ion battery. *Electrochimica Acta*, 116:300–305, 2014.

[26] Yihang Liu, Xin Fang, Anyi Zhang, Chenfei Shen, Qingzhou Liu, Hani A Enaya, and Chongwu Zhou. Layered p2-$Na_{2/3}[Ni_{1/3}Mn_{2/3}]O_2$ as high-voltage cathode for sodium-ion batteries: the capacity decay mechanism and Al_2O_3 surface modification. *Nano Energy*, 27:27–34, 2016.

[27] Karthikeyan Kaliyappan, Jian Liu, Biwei Xiao, Andrew Lushington, Ruying Li, Tsun-Kong Sham, and Xueliang Sun. Enhanced performance of p2-$Na_{0.66}(Mn_{0.54}Co_{0.13}Ni_{0.13})O_2$ cathode for sodium-ion batteries by ultrathin metal oxide coatings via atomic layer deposition. *Advanced Functional Materials*, 27(37):1701870, 2017.

[28] Hari Vignesh Ramasamy, Karthikeyan Kaliyappan, Ranjith Thangavel, Vanchiappan Aravindan, Kisuk Kang, Dae Ung Kim, Yongll Park, Xueliang Sun, and Yun-Sung Lee. Cu-doped p2-$Na_{0.5}Ni_{0.33}Mn_{0.67}O_2$ encapsulated with MgO as a novel high voltage cathode with enhanced na-storage properties. *Journal of materials Chemistry A*, 5(18):8408–8415, 2017.

[29] Yang Yu, Weijin Kong, Qingyuan Li, De Ning, Gotz Schuck, Gerhard Schumacher, Chunjian Su, and Xiangfeng Liu. Understanding the multiple effects of TiO_2 coating on $NaMn_{0.33}Fe_{0.33}Ni_{0.33}O_2$ cathode material for na-ion batteries. *ACS Applied Energy Materials*, 3(1):933–942, 2020.

[30] Shuo Bao, Shao-Hua Luo, and Jin-Lin Lu. Preparation and optimization of ZrO_2 modified p2-type $Na_{2/3}Ni_{1/6}Co_{1/6}Mn_{2/3}O_2$ with enhanced electrochemical performance as cathode for sodium ion batteries. *Ceramics International*, 46(10):16080–16087, 2020.

[31] Yu Wang, Ke Tang, Xiaolong Li, Ruizhi Yu, Xiaohui Zhang, Yan Huang, Gairong Chen, Sidra Jamil, Shuang Cao, Xin Xie, et al. Improved cycle and air stability of p3-$Na_{0.65}Mn_{0.75}Ni_{0.25}O_2$ electrode for sodium-ion batteries coated with metal phosphates. *Chemical Engineering Journal*, 372:1066–1076, 2019.

[32] Karthikeyan Kaliyappan, Tyler Or, Ya-Ping Deng, Yongfeng Hu, Zhengyu Bai, and Zhongwei Chen. Constructing safe and durable high-voltage p2 layered cathodes for sodium ion batteries enabled by molecular layer deposition of alucone. *Advanced Functional Materials*, 30(17):1910251, 2020.

[33] Ya You, Sen Xin, Hooman Yaghoobnejad Asl, Wangda Li, Peng-Fei Wang, Yu-Guo Guo, and Arumugam Manthiram. Insights into the improved high-voltage performance of li-incorporated layered oxide cathodes for sodium-ion batteries. *Chem*, 4(9):2124–2139, 2018.

[34] James W Somerville, Adam Sobkowiak, Nuria Tapia-Ruiz, Juliette Billaud, Juan G Lozano, Robert A House, Leighanne C Gallington, Tore Ericsson, Lennart Häggström, Matthew R Roberts, et al. Nature of the "z"-phase in layered na-ion battery cathodes. *Energy & Environmental Science*, 12(7):2223–2232, 2019.

[35] Pete Barnes, Kassiopeia Smith, Riley Parrish, Chris Jones, Paige Skinner, Erik Storch, Quinn White, Changjian Deng, Devan Karsann, Miu Lun Lau, et al. A non-aqueous sodium hexafluorophosphate-based electrolyte degradation study: Formation and mitigation of hydrofluoric acid. *Journal of Power Sources*, 447:227363, 2020.

[36] R Prasad, R Benedek, and MM Thackeray. Dopant-induced stabilization of rhombohedral $LiMnO_2$ against jahn-teller distortion. *Physical Review B*, 71(13):134111, 2005.

[37] Ji Ung Choi, Yun Ji Park, Jae Hyeon Jo, Liang-Yin Kuo, Payam Kaghazchi, and Seung-Taek Myung. Unraveling the role of earth-abundant fe in the suppression of jahn-teller distortion of p′2-type $Na_{2/3}MnO_2$: experimental and theoretical studies. *ACS applied materials & interfaces*, 10(48):40978–40984, 2018.

[38] Bachu Sravan Kumar, Anagha Pradeep, Animesh Dutta, and Amartya Mukhopadhyay. Water-stable o3-type layered na transition metal oxides enabling environment friendly aqueous processing of electrodes with long-term electrochemical stability. *Journal of Materials Chemistry A*, 8(35):18064–18078, 2020.

[39] Maider Zarrabeitia, Elena Gonzalo, Marta Pasqualini, Matteo Ciambezi, Oier Lakuntza, Francesco Nobili, Angela Trapananti, Andrea Di Cicco, Giuliana Aquilanti, Nebil A Katcho, et al. Unraveling the role of ti in the stability of positive layered oxide electrodes for rechargeable na-ion batteries. *Journal of Materials Chemistry A*, 7(23):14169–14179, 2019.

[40] Wenhua Zuo, Jimin Qiu, Xiangsi Liu, Fucheng Ren, Haodong Liu, Huajin He, Chong Luo, Jialin Li, Gregorio F Ortiz, Huanan Duan, et al. The stability of p2-layered sodium transition metal oxides in ambient atmospheres. *Nature communications*, 11(1):1–12, 2020.

[41] Yuqi Li, Yang Yang, Yaxiang Lu, Quan Zhou, Xingguo Qi, Qingshi Meng, Xiaohui Rong, Liquan Chen, and Yong-Sheng Hu. Ultralow-concentration electrolyte for na-ion batteries. *ACS Energy Letters*, 5(4):1156–1158, 2020.

[42] Yan Jin, Yaobin Xu, Phung ML Le, Thanh D Vo, Quan Zhou, Xingguo Qi, Mark H Engelhard, Bethany E Matthews, Hao Jia, Zimin Nie, et al. Highly reversible sodium ion batteries enabled by stable electrolyte-electrode interphases. *ACS Energy Letters*, 5(10):3212–3220, 2020.

[43] Yuesheng Wang, Zimin Feng, Peixin Cui, Wen Zhu, Yue Gong, Marc-André Girard, Gilles Lajoie, Julie Trottier, Qinghua Zhang, Lin Gu, et al. Pillar-beam structures prevent layered cathode materials from destructive phase transitions. *Nature Communications*, 12(1):1–11, 2021.

[44] Xiaohui Rong, Enyuan Hu, Yaxiang Lu, Fanqi Meng, Chenglong Zhao, Xuelong Wang, Qinghua Zhang, Xiqian Yu, Lin Gu, Yong-Sheng Hu, et al. Anionic redox reaction-induced high-capacity and low-strain cathode with suppressed phase transition. *Joule*, 3(2):503–517, 2019.

[45] Ling Li, Huibo Wang, Wenze Han, Hao Guo, Andreas Hoser, Yujun Chai, and Xiangfeng Liu. Understanding oxygen redox in cu-doped p2-$Na_{0.67}Mn_{0.8}Fe_{0.1}Co_{0.1}O_2$ cathode materials for na-ion batteries. *Journal of The Electrochemical Society*, 165(16):A3854, 2018.

[46] Lufeng Yang, Xiang Li, Jue Liu, Shan Xiong, Xuetian Ma, Pan Liu, Jianming Bai, Wenqian Xu, Yuanzhi Tang, Yan-Yan Hu, et al. Lithium-doping stabilized high-performance p2-$Na_{0.66}Li_{0.18}Fe_{0.12}Mn_{0.7}O_2$ cathode for sodium ion batteries. *Journal of the American Chemical Society*, 141(16):6680–6689, 2019.

[47] Ivana Hasa, Stefano Passerini, and Jusef Hassoun. Toward high energy density cathode materials for sodium-ion batteries: investigating the beneficial effect of aluminum doping on the p2-type structure. *Journal of Materials Chemistry A*, 5(9):4467–4477, 2017.

[48] Ding Zhang, Xiao-Meng Meng, Ya-Min Zheng, Xiao-Min Wang, Shou-Dong Xu, Liang Chen, and Shi-Bin Liu. The critical role of titanium cation in the enhanced performance of p2-$Na_{0.5}Ni_{0.25}Mn_{0.60}Ti_{0.15}O_2$ cathode material for sodium-ion batteries. *Physical Chemistry Chemical Physics*, 22(35):19992–19998, 2020.

[49] Qianjiang Mao, Cheng Zhang, Wenyun Yang, Jinbo Yang, Limei Sun, Yongmei Hao, and Xiangfeng Liu. Mitigating the voltage fading and lattice cell variations of o3-$NaNi_{0.2}Fe_{0.35}Mn_{0.45}O_2$ for high performance na-ion battery cathode by zn doping. *Journal of Alloys and Compounds*, 794:509–517, 2019.

[50] Zheng-Yao Li, Rui Gao, Limei Sun, Zhongbo Hu, and Xiangfeng Liu. Zr-doped p2-$Na_{0.75}Mn_{0.55}Ni_{0.25}Co_{0.05}Fe_{0.10}Zr_{0.05}O_2$ as high-rate performance cathode material for sodium ion batteries. *Electrochimica Acta*, 223:92–99, 2017.

[51] Jae Hyeon Jo, Ji Ung Choi, Aishuak Konarov, Hitoshi Yashiro, Shuai Yuan, Liyi Shi, Yang-Kook Sun, and Seung-Taek Myung. Sodium-ion batteries: Building effective layered cathode materials with long-term cycling by modifying the surface via sodium phosphate. *Advanced Functional Materials*, 28(14):1705968, 2018.

[52] Kai Liu, Qingqing Zhang, Sheng Dai, Wei Li, Xingjiang Liu, Fei Ding, and Jinli Zhang. Synergistic effect of f–doping and lif coating on improving the high-voltage cycling stability and rate capacity of $LiNi_{0.5}Co_{0.2}Mn_{0.3}O_2$ cathode materials for lithium-ion batteries. *ACS applied materials & interfaces*, 10(40):34153–34162, 2018.

[53] Linze Li, Zhengyan Lun, Dongchang Chen, Yuan Yue, Wei Tong, Guoying Chen, Gerbrand Ceder, and Chongmin Wang. Fluorination-enhanced surface stability of cation-disordered rocksalt cathodes for li-ion batteries. *Advanced Functional Materials*, page 2101888, 2021.

[54] Bing Zhao, Jian Si, Chunhui Cao, Jian Zhang, Baojia Xia, Jingwei Xie, Bobo Li, and Yong Jiang. Enhanced electrochemical performance of $LiNi_{0.8}Co_{0.15}Al_{0.05}O_2$ cathode by reducing lithium residue with low-temperature fluorination treatment. *Solid State Ionics*, 339:114998, 2019.

[55] Susumu Yonezawa, Masahiro Yamasaki, and Masayuki Takashima. Surface fluorination of the cathode active materials for lithium secondary battery. *Journal of fluorine chemistry*, 125(11):1657–1661, 2004.

[56] Ulf Breddemann, Evan M Erickson, Victoria Davis, Florian Schipper, Mathias Ellwanger, Michael Daub, Anke Hoffmann, Christoph Erk, Boris Markovsky, Doron Aurbach, et al. Fluorination of li-rich lithium-ion-battery cathode materials by fluorine gas: Chemistry, characterization, and electrochemical performance in half cells. *ChemElectroChem*, 6(13):3337–3349, 2019.

[57] Mukul D Tikekar, Snehashis Choudhury, Zhengyuan Tu, and Lynden A Archer. Design principles for electrolytes and interfaces for stable lithium-metal batteries. *Nature Energy*, 1(9):1–7, 2016.

[58] Lili Wang, Shiyang Fu, Teng Zhao, Ji Qian, Nan Chen, Li Li, Feng Wu, and Renjie Chen. In situ formation of a lif and li–al alloy anode protected layer on a li metal anode with enhanced cycle life. *Journal of Materials Chemistry A*, 8(3):1247–1253, 2020.

[59] Dingchang Lin, Yayuan Liu, Wei Chen, Guangmin Zhou, Kai Liu, Bruce Dunn, and Yi Cui. Conformal lithium fluoride protection layer on three-dimensional lithium by nonhazardous gaseous reagent freon. *Nano letters*, 17(6):3731–3737, 2017.

[60] Shiqiang Huang, Shuwei Wang, Guohong Hu, Ling-Zhi Cheong, and Cai Shen. Modulation of solid electrolyte interphase of lithium-ion batteries by lidfob and libob electrolyte additives. *Applied Surface Science*, 441:265–271, 2018.

[61] Robert A House, Urmimala Maitra, Miguel A Pérez-Osorio, Juan G Lozano, Liyu Jin, James W Somerville, Laurent C Duda, Abhishek Nag, Andrew Walters, Ke-Jin Zhou, et al. Superstructure control of first-cycle voltage hysteresis in oxygen-redox cathodes. *Nature*, 577(7791):502–508, 2020.

Appendix A

SUPPLEMENTARY DATA

The charge discharge curve for half-cell NFM cathode having glass fiber as separator at 0.1 C at 25°C.

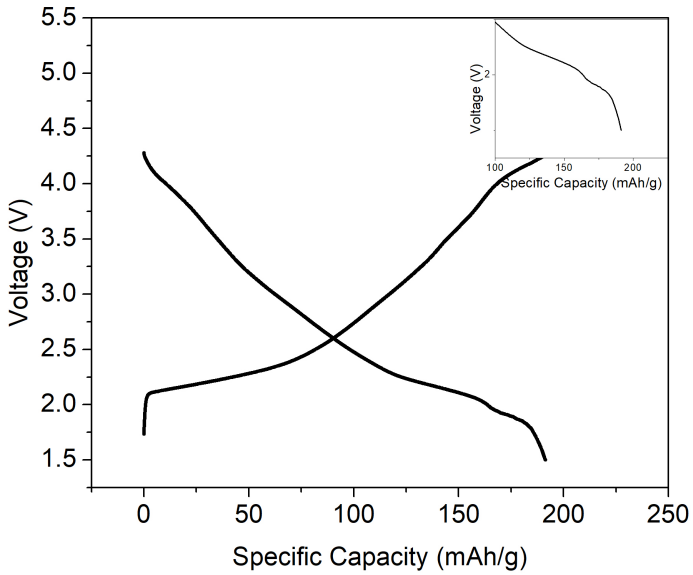

Figure A.1: Charge discharge curve for first cycle of NFM vs. Na. The inset shows low voltage electrochemical transition which was absent when other separators were used